7. From Radiation Fields to Atmospheric Concentrations – Retrieval of Geophysical Parameters

H. Bovensmann[1], A. Doicu[2], P. Stammes[3], M. Van Roozendael[4], C. von Savigny[1], M. Penning de Vries[5], S. Beirle[5], T. Wagner[5], K. Chance[6], M. Buchwitz[1], A. Kokhanovsky[1], A. Richter[1], A.V. Rozanov[1], V.V. Rozanov[1],

[1] Institute of Environmental Physics / Institute of Remote Sensing (IUP-IFE), University of Bremen, Otto-Hahn-Allee 1, 28359 Bremen, Germany
[2] Remote Sensing Technology Institute, German Aerospace Center (DLR-IMF), Oberpfaffenhofen, 82234 Wessling, Germany
[3] Royal Netherlands Meteorological Institute (KNMI), Wilhelminalaan 10, 3732 GK De Bilt, The Netherlands
[4] Belgian Institute for Space Aeronomie (BIRA-IASB), 3 Avenue Circulaire, 1180 Brussels, Belgium
[5] Max Planck Institute for Chemistry, Johann-Joachim-Becher-Weg 27, 55128 Mainz, Germany
[6] Harvard-Smithsonian Center for Astrophysics (SAO), 60 Garden Street, Cambridge, MA 02138, USA

Abstract: Satellite-based atmospheric remote sensing aims at deriving the properties of trace gases, aerosols and clouds, as well as surface parameters from the measured top-of-atmosphere spectral radiance and reflectance. This requires, besides high quality spectra, an accurate modelling of the radiative transfer of solar radiation through the atmosphere to the sensor (*forward model*), and methods to derive the constituent properties from the measured top-of-atmosphere spectra (*inversion methods*). Many trace gases have structured absorption spectra in the UV-VIS spectral range serving as the starting point for determining their abundance by applying Differential Optical Absorption Spectroscopy (DOAS) or similar methods. In the UV-VIS-NIR and SWIR spectral regions, the solar radiation is strongly scattered by clouds and aerosols. Therefore, the presence of clouds and aerosol particles and their properties can also be inferred from the outgoing radiance measured by space-based instruments. Contrary to the forward model, the inversion methods allow to derive characteristics of the atmospheric state based on the measured quantities. A common product of the inversion of satellite measurements in limb, nadir or occultation geometry are total columns or height-resolved profiles of trace gas concentrations and aerosol parameters. Retrieving trace gas amounts in the troposphere constitutes a specific challenge. SCIAMACHY's unique limb/nadir matching capability provides access to tropospheric columns by combining total columns obtained from nadir geometry with simultaneously measured stratospheric columns obtained from limb geometry.

Keywords: Atmospheric composition retrieval – Absorption – Scattering – Radiative transfer – Differential Optical Absorption Spectroscopy (DOAS) – Inversion theory

Satellite remote sensing of the atmosphere with spectrometers such as SCIAMACHY gives the top-of-atmosphere (TOA) spectral radiance. It remains a challenging task to quantitatively derive the atmospheric composition – trace gases, aerosols, clouds – from these measurements. The main source of radiation for passive remote sounding of the atmosphere by SCIAMACHY in the UV-SWIR regions is the Sun. The absorption and scattering characteristics of the Earth's atmosphere can be determined by comparing the radiance reflected from the Earth's surface and scattered by the atmosphere to the sensor with the unaffected extraterrestrial solar irradiance entering at the top of the atmosphere. A quantitative analysis requires:

- Earth and solar radiance spectra of high spectral and radiometric quality
- An accurate modelling of the transfer of the solar light through the atmosphere to the sensor (*radiative transfer model* or *forward model*), and

– Techniques to relate the measured TOA spectra to the constituent properties (usually referred to as *inversion methods*).

The retrieval of information on atmospheric trace gases relies on the knowledge of the absorption, emission and scattering of electromagnetic radiation in the atmosphere. In the UV-VIS-NIR and SWIR spectral ranges, the radiative transfer through the atmosphere is affected by (see Fig. 7-1):

– Scattering by air molecules (Rayleigh and Raman scattering)
– Scattering and absorption by aerosol and cloud particles (Mie scattering)
– Absorption and emission by trace gases
– Refraction due to the density gradient in the atmosphere
– Surface reflection and absorption.

These are the processes which must be quantitatively taken into account when retrieving atmospheric geophysical parameters from SCIAMACHY measurements.

Trace gases usually exhibit characteristic fingerprint spectra in emission or absorption, originating from:

– Rotational transitions: primarily observed in the far infrared and microwave spectral regions
– Vibrational-rotational transitions: can be measured in the thermal and short-wave infrared
– Electronic transitions: mainly detected in the UV-VIS and NIR spectral regions.

SCIAMACHY with its wide spectral coverage from the UV to the SWIR detects trace gases mainly via their electronic and vibrational-rotational transition spectra.

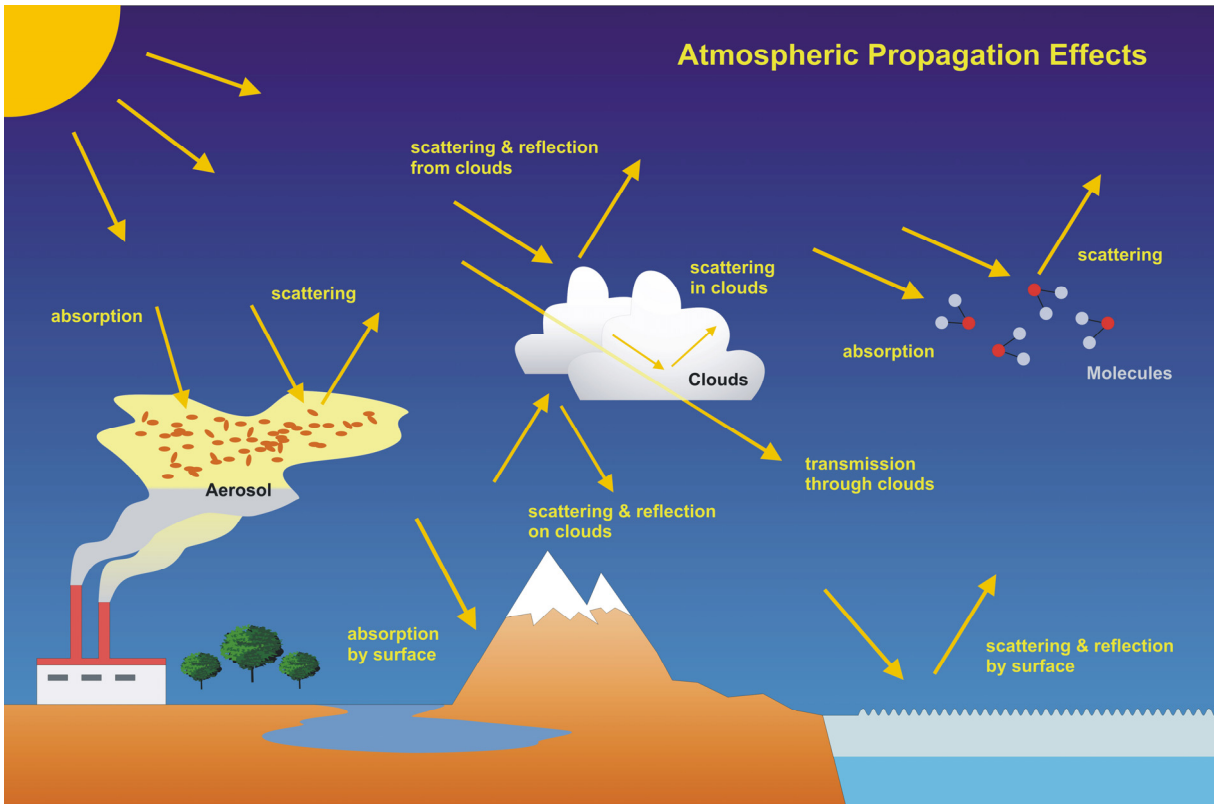

Fig. 7-1: Scheme of the relevant interactions of solar light with the Earth's atmosphere and surface. (Courtesy: DLR-IMF)

7.1 Radiative Transfer in the Earth's Atmosphere

Important tools to simulate changes in the solar radiation due to atmospheric scattering and absorption processes are radiative transfer models (RTM), also referred to as *forward models*. They provide the synthetic radiances, as they would be measured by the sensor, for a specified state of the atmosphere. These models are an important part of any retrieval process. Considering the entire atmosphere, one usually talks about the radiation field, which describes the angular and spatial distribution of the radiation in the atmosphere.

The main characteristic of the radiation field in the atmosphere is the radiance I (also often referred to as 'intensity'), which is defined as the flux of energy in a given direction per unit time per unit wavelength range per unit solid angle per unit area perpendicular to a given direction (Liou 2002). All interactions between the radiation and the atmosphere are classified by the sign of the change of the radiation intensity as a result of the interaction. Processes which reduce the intensity in the direction under consideration by absorption, as well as scattering processes from the original direction into other directions, are commonly named *extinction*. Processes which increase the intensity in the direction under consideration, for example by scattering into the beam from other directions, by thermal or other emission processes within the volume, are referred to as *source function*.

In the description of radiative transfer presented here we neglect the polarisation state of light for reasons of simplicity. However, we note that polarisation is important for SCIAMACHY for two reasons, namely in order to

- Accurately simulate radiances in the UV and VIS
- Account for the polarisation sensitivity of the instrument when determining the true radiance (see discussion in chapter 5).

The general form of the radiative transfer equation describes all processes affecting the radiation field as a result of its interaction with a medium, taking energy conservation into account. It has the form

$$\frac{dI}{ds} = -\alpha (I - J) \tag{7-1}$$

where I is radiance (or intensity) in a given direction, s the light path, α is the extinction coefficient describing the fraction of the energy which is removed from the original beam by absorption and scattering, and J is the source function which describes the increase of the radiance I into the original direction due to scattering and/or emission.

If the amount of light travelling in a certain direction through the atmosphere can only be increased due to the scattering processes – as is the case for the spectral range covered by SCIAMACHY when neglecting emissions – the source function depends on the intensity falling on the elementary volume from all directions

$$J = \frac{\omega}{4\pi} \int p(\gamma)\, I\, d\Omega \tag{7-2}$$

with γ being the scattering angle, i.e. the angle between the directions of the incident and scattered radiation, and ω is the single scattering albedo representing the probability that a photon, which interacts with a volume element, will be scattered rather than being absorbed. The term $p(\gamma)d\Omega/4\pi$ denotes the probability that the radiation is scattered into a solid angle $d\Omega$ about a direction forming an angle γ with the direction of the incident radiation. The quantity $p(\gamma)$ is called the phase function.

The total radiation field can be split into two components

$$I = I_{dir} + I_{dif} \tag{7-3}$$

with I_{dir} being the direct radiation, which is never scattered in the atmosphere or reflected from the Earth's surface, and the diffuse radiation I_{dif}, which is scattered or reflected at least once. Since there is

no relevant process in the atmosphere which increases the intensity of the direct solar radiation, the radiative transfer equation for the direct radiation leads to the homogeneous differential equation

$$\frac{dI_{dir}}{ds} = -\alpha I_{dir} \tag{7-4}$$

with a solution described by Lambert-Beer's law

$$I_{dir} = I_0 \exp\left(-\int \alpha(s)\, ds\right) \tag{7-5}$$

where I_0 being the incident radiance at the top of the atmosphere, which is described – assuming the Sun has an infinitesimal size – by the solar irradiance I_{irr} multiplied by the Dirac delta-function (see, e.g. Thomas and Stamnes 1999). The integral $\int \alpha(s) ds$ along the photon path defines the *optical depth* $\tau(s)$. Integration is performed along the direct solar beam from the surface to the top-of-atmosphere. This equation describes the attenuation of the direct solar or lunar light travelling through the atmosphere. Thus, the direct component (7-5) is a good approximation for the radiative transfer when directly viewing the Sun or the Moon, for example. Therefore, it can be used to describe SCIAMACHY measurements in occultation geometry.

If the diffuse radiation is non-negligible – as for SCIAMACHY nadir and limb measurements – it has to be considered in addition to the direct one. The corresponding radiative transfer equation (7-1) for the diffuse component using the scattering source function (7-2) can be written then as follows (details see Liou 2002):

$$\frac{dI_{dif}}{ds} = -\alpha\left(I_{dif} - \frac{\omega}{4\pi}\int p(\gamma)\, I_{dif}\, d\Omega - \frac{\omega}{4\pi}\, p(\gamma_0) I_{irr} \exp\left(-\int \alpha(s) ds\right)\right) \tag{7-6}$$

where γ_o denotes the scattering angle between the direct solar beam and the direction of observation, and I_{irr} is the extraterrestrial solar flux, often also termed 'irradiance'. Various standard methods to solve (7-6) are presented in Lenoble (1985) or Liou (2002).

Light is scattered by atoms and molecules, as well as by various types of aerosols and clouds. Molecular scattering cross sections are characterised by the Rayleigh law (λ^{-4}), whereas aerosol scattering typically shows a much less pronounced dependence on wavelength with about λ^{-1} (Mie scattering). For cloud-free scenes, molecular scattering usually dominates in the UV spectral range, while aerosols become more important in the VIS and NIR range (see also Fig. 7-3). The molecular scattering consists of two parts: the elastic Rayleigh component which accounts for about 96% of scattering events, and the 4% inelastic rotational Raman component which is responsible for the *Ring* effect, the 'filling in' of solar Fraunhofer lines in the registered earthshine spectra (Grainger and Ring 1962). Further details on atmospheric radiative transfer can be found in e.g. Liou (2002).

As an example, Fig. 7-2 shows the solar irradiance spectrum and the backscattered radiance at the top-of-atmosphere. When SCIAMACHY nadir radiances at high solar zenith angles SZA > 75° are simulated, the sphericity of the atmosphere must be taken into account when calculating the attenuation of the direct solar light. For simulating SCIAMACHY limb radiances, both the direct and the diffuse radiance have to be treated in a spherical atmosphere, including refraction. The numerical solution of the radiative transfer equation is then accomplished, e.g. by an iterative approach (Rozanov et al. 2001). Depending on the scientific application, several radiative transfer models are used in the SCIAMACHY data analysis. These are GOMETRAN/SCIATRAN (Rozanov et al. 1998, 2005a), LIDORT (Linearized Discrete Ordinate Radiative Transfer, Spurr et al. 2001), DAK (Doubling-Adding KNMI, Stammes 2001), SCIARAYS (Kaiser and Burrows 2003), VECTOR (McLinden et al. 2002), and McArtim (Monte Carlo Atmospheric Radiative Transfer Inversion Model, Deutschmann et al. 2010). These radiative transfer models are not only able to simulate the radiance measured by SCIAMACHY, but also to deliver additional parameters to quantify and characterise the geophysical parameters of interest. One of these parameters is the *weighting function*. This function is the derivative of the modelled radiance with respect to a selected parameter, describing how the radiance changes when this parameter is modified. Another important quantity to be delivered by radiative

transfer models is the *Air Mass Factor* (AMF, see chapter 7.2) which provides a measure for the average photon path length in the atmosphere under optically thin conditions (optical depth << 1).

The quality of the radiative transfer simulation results is often assessed in application-specific radiative transfer model inter-comparison exercises. This was done for example for limb radiative transfer applications by Loughman et al. (2004), for the AMF by Wagner et al. (2007a,) and for polarised radiative transfer calculations by Kokhanovsky et al. (2010).

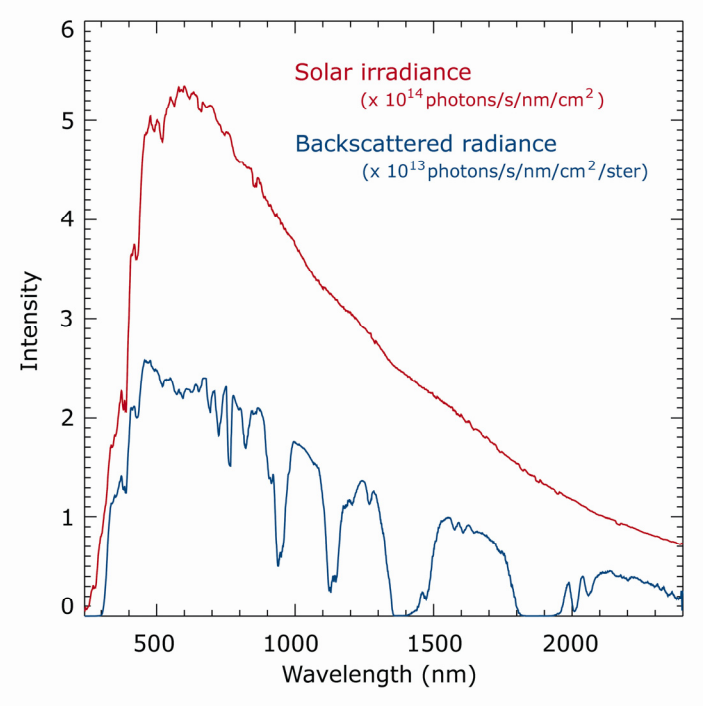

Fig. 7-2: The solar irradiance spectrum (red) and Earth radiance spectrum (blue) with a shape modified by absorption of trace gases and scattering in the atmosphere. (Courtesy: IUP-IFE, University of Bremen)

7.2 Nadir Trace Gas Retrieval Schemes

DOAS Retrieval

Many molecules of atmospheric relevance have structured absorption spectra in the UV-VIS and NIR spectral range (Fig. 7-3). These can be used to determine the total atmospheric abundance of the species from remote sensing measurements of scattered sunlight using *inverse methods* (see also chapter 7.5), which relate the measured atmospheric spectra to the constituent properties in the atmosphere. One powerful and intuitive approach is the Differential Optical Absorption Spectroscopy (DOAS), originally developed for ground-based measurements using artificial light sources or scattered sunlight (Noxon 1975, Platt et al. 1979, Solomon et al. 1987, Platt and Stutz 2008) and successfully adapted to nadir – and partly limb – measurements from GOME, SCIAMACHY, OMI and GOME-2 (Richter and Wagner 2010). Two main ideas form the basis of the DOAS approach (Fig. 7-4):

- The isolation of high frequency structures of molecular absorbers from broadband scattering features (Rayleigh, Mie) by a high pass filter.
- The separation of spectroscopic retrievals and radiative transfer calculations using the Air Mass Factor (AMF) concept.

Given a measured spectrum $I_{abs}(\lambda)$ containing the absorption of the trace gas of interest, a reference spectrum without the absorption of the trace gas of interest $I_{ref}(\lambda)$ and the absorption cross sections $\sigma_i(\lambda)$ of all relevant species, the optical depth can be written according to Lambert-Beer's law (7-5). Under the assumption of an optically thin atmosphere in the spectral region of interest, this optical depth is approximated as described in (7-7), where it is also assumed that the pressure and temperature dependence of the absorption cross sections can be neglected:

$$\tau_s(\lambda) = -\ln\left(\frac{I_{abs}(\lambda)}{I_{ref}(\lambda)}\right) \approx \sum_i \sigma_i(\lambda) SCD_i(\lambda) - \sum_j c_j \lambda^j \tag{7-7}$$

For $I_{abs}(\lambda)$ the nadir or limb radiance $I(\lambda)$ measured by SCIAMACHY is used. For $I_{ref}(\lambda)$ an extra-terrestrial solar spectrum determined from SCIAMACHY's solar measurements is applied. Alternatively, nadir or limb spectra from regions where the absorber of interest shows negligible absorptions are used. While molecular absorption cross sections $\sigma_i(\lambda)$ are usually highly structured, absorption by particles, scattering by molecules and particles, as well as reflection at the surface show broadband dependences. These broadband modulations are approximated in the DOAS approach by a common polynomial of low order with polynomial coefficients c_j. The slant column density SCD_i is the molecular number density n_i integrated along the light path s:

$$SCD_i(\lambda) = \int n_i(s) ds(\lambda) \tag{7-8}$$

The spectral fit window is selected in such a way that the trace gas of interest shows strong and characteristic absorption features. The SCD_i is then obtained using a linear least squares fit by minimising the following quadratic form, where the wavelength dependence of the SCD is omitted to simplify the expression to

$$\left\| \tau_s(\lambda) - \sum_i \sigma_i(\lambda) SCD_i + \sum_j c_j \lambda^j \right\|^2 \tag{7-9}$$

Fit parameters are the slant column densities SCD_i and the polynomial coefficients c_j. Fig. 7-5 depicts a typical fit for NO_2. Once the SCD_i have been determined from the measured spectra, the conversion to the desired vertical column densities VCD_i is the last step. This requires for each trace gas a division by the Air Mass Factor (AMF_i) according to

$$VCD_i = \int n_i(z) dz = SCD_i / AMF_i \tag{7-10}$$

with $n_i(z)$ being the vertical number density profile of the i-th absorber. The AMF describes the sensitivity of the measurement related to the specific properties of the atmospheric light path. Besides the solar elevation, the AMF depends on the measurement geometry and on the vertical profiles of absorbing and scattering constituents in the atmosphere as well as on the surface spectral reflectance. The AMF is calculated with a radiative transfer model and is essentially the ratio of the logarithms of atmospheric radiances simulated including all trace gases and excluding the trace gas of interest (Sarkissian et al. 1995, Burrows et al. 1999, Rozanov and Rozanov 2010). RTM calculations require trace gas profiles as input which are taken from climatologies or chemical transport models. The effect of partial cloudiness of the scene can be accounted for in the AMF calculation (Burrows et al. 1999). Radiative transfer models are also used to extend the AMF concept to a so-called 'box-AMF' concept, allowing for a height-dependent assessment of the sensitivity of DOAS measurements (Wagner et al. 2007a). The box-AMF characterises the ratio of the partial slant column density (SCD_{box}) to the partial vertical column density (VCD_{box}) of an atmospheric layer. It has to be noted, that for optically thin absorbers (optical depth <<1), the box-AMFs are proportional to the weighting functions.

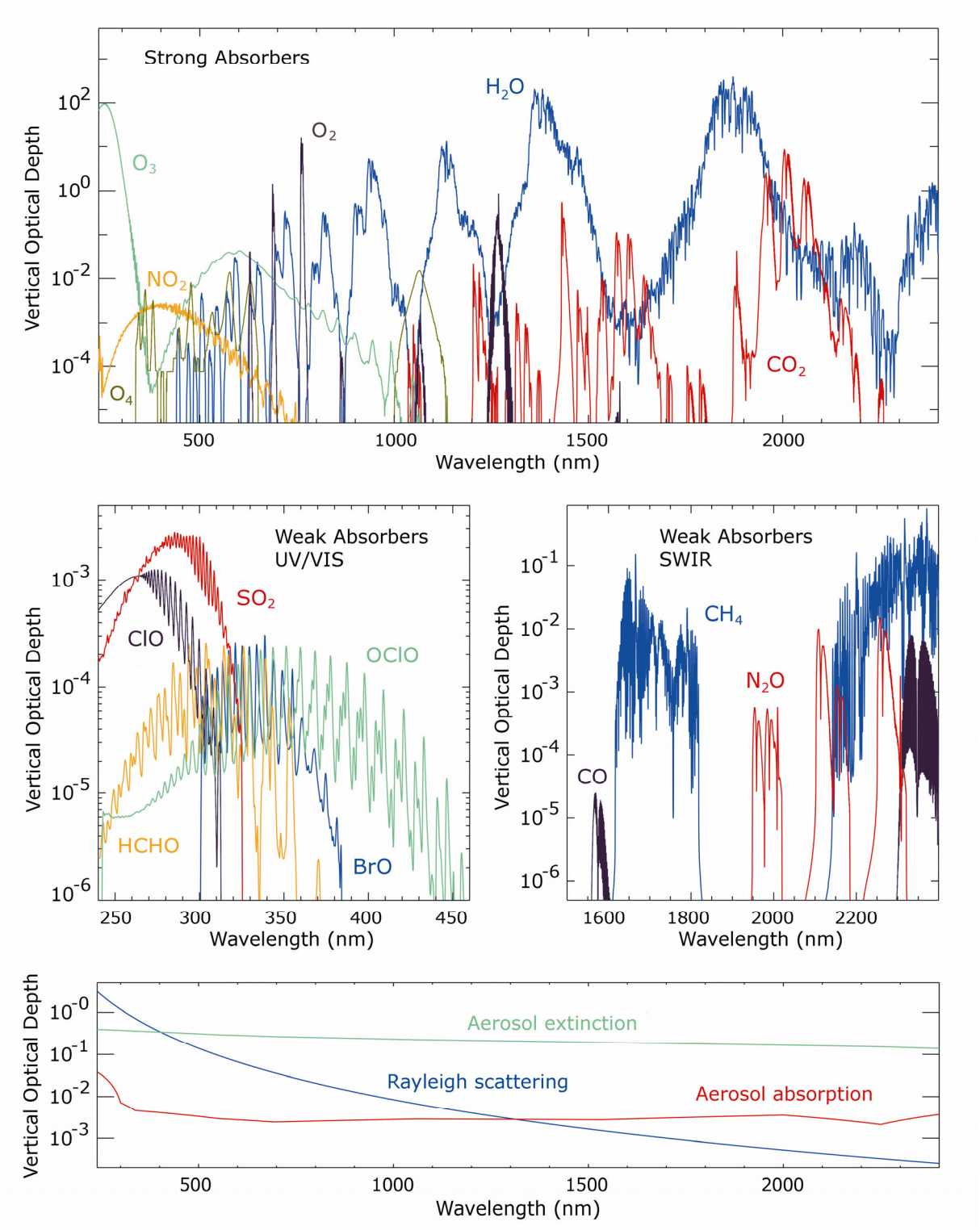

Fig. 7-3: Simulated vertical optical depth of the targeted constituents for 55°N around 10 a.m. The strong absorbers are plotted in the upper part and the relevant weak absorbers in the middle part. In the lower part, the vertical optical depth due to Rayleigh scattering, aerosol extinction and absorption is given. Note the large dynamic range of the differential absorption structures used for retrieval of the constituents. (Courtesy: IUP-IFE, University of Bremen)

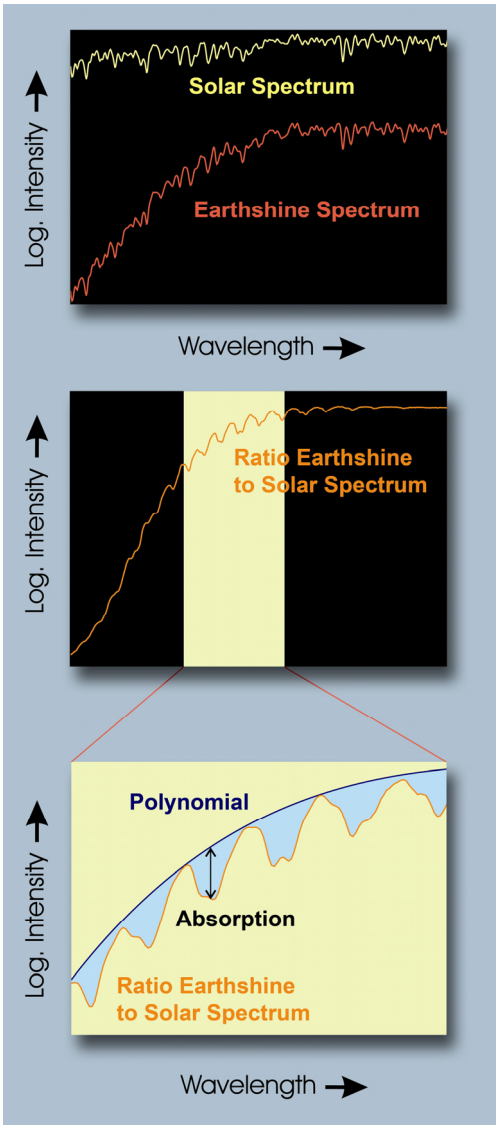

Fig. 7-4: The main steps of the DOAS retrieval. For further details see the text. (Courtesy: IUP-IFE, University of Bremen)

The quality of the DOAS analysis is affected by the accuracies achieved in the slant column spectral fitting procedure as well as in the AMF calculation. The slant column spectral fitting is, especially for weak absorbing trace gases, a challenge in itself - not only for DOAS but also for other inverse methods described below – as very tiny spectral structures (amplitude of a few 10^{-4}) need to be quantitatively separated from interfering spectral structures. The performance of the slant column fitting is mainly driven by the signal-to-noise ratio (SNR) of the measurement, spectral calibration and knowledge of the instrument slit function, the separation of interfering spectral structures, the separation of the Ring effect and how one corrects for imperfect spectral sampling (Chance 1998). This imperfect sampling, which is a common feature in atmospheric UV-VIS spectra taken by current spaceborne spectrometers, may cause significant systematic spectral structures in the fitting process. For example, undersampled spectra cannot be re-sampled in wavelength without introducing spurious features due to spectral aliasing. Such structures introduced by aliasing can be largely corrected in the case where atmospheric absorptions are optically thin by calculating an undersampling correction using an independent, high resolution, solar reference spectrum (see also Slijkhuis et al. 1999, Chance et al. 2005).

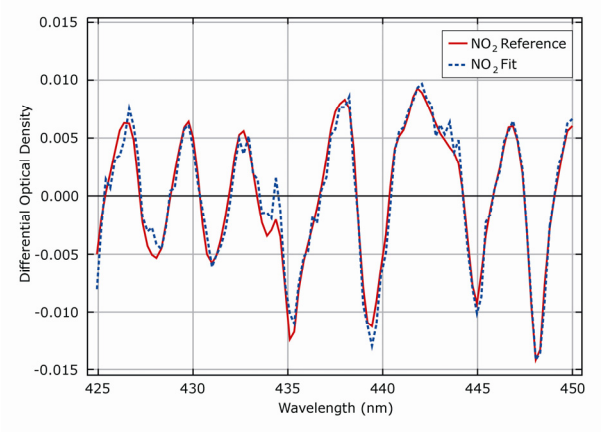

Fig. 7-5: Typical SCIAMACHY NO_2 fit results from a measurement over a polluted area in China on 15 January 2006. The red line is the scaled NO_2 laboratory cross section, the dashed blue line the result of the fit after subtraction of all contributions with the exception of NO_2. (Courtesy: IUP-IFE, University of Bremen)

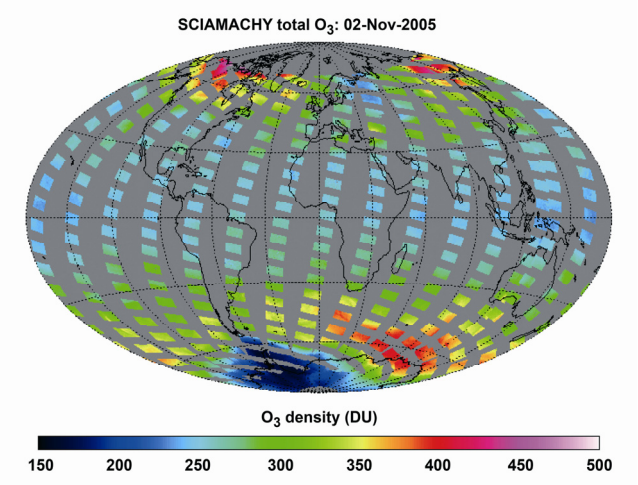

Fig. 7-6: One day of total ozone densities obtained with the TOSOMI algorithm. (Courtesy: KNMI/ESA)

Rayleigh scattering is partially inelastic as manifested via the Ring effect. The inelastic component is Raman scattering by air molecules, predominantly rotational Raman scattering. It varies from 4.0% to 3.4% of the total scattering over the wavelength region of 280-1000 nm (Bates 1984, Chance and Spurr 1997). Thus, to first order, the correction for the Ring effect in atmospheric spectra is simply the convolution of the solar irradiance with the spectrum of Raman scattering by air. In the DOAS slant column fitting procedure, the Ring effect is taken into account as an additional 'absorber' with an effective cross section $\sigma_{Ring}(\lambda)$ as originally proposed by Solomon et al. (1987). Examples how to determine this cross section can be found in Chance and Spurr (1997), Vountas et al. (1998) and Wagner et al. (2009).

When calculating the AMF, accuracy depends on the knowledge of the main parameters determining the radiative transfer in the atmosphere, i.e. clouds, aerosols, surface spectral reflectance, surface elevation, height dependence of absorbers and scatterers. Obviously, clouds drastically modify the light path through the atmosphere and need to be properly taken into account when calculating the AMF (see chapter 7.3). The most important cloud parameters are the cloud fraction and the cloud top altitude, as fractional cloudiness blocks the light path to atmospheric layers below the cloud. The optical thickness of clouds also plays a role.

Using the DOAS algorithm, atmospheric columns of a number of species can be determined, including O_3, NO_2, SO_2, HCHO, CHOCHO, BrO, IO and OClO. For details, see Table 7-1 and references therein.

Modified DOAS Methods

One limitation of the classical DOAS technique is the assumption that the atmosphere is optically thin in the wavelength region of interest. In addition, 'line-absorbers' such as H_2O, O_2, CO, CO_2 and CH_4 usually cannot be retrieved precisely by standard DOAS algorithms because their strong absorption also depends on pressure and temperature and their spectra are often not fully spectrally resolved by SCIAMACHY. To overcome these drawbacks, several DOAS-type techniques were developed to

account for such effects and to permit successful retrievals of the trace gas species (for a theoretical overview see Rozanov and Rozanov 2010). They are, for example, the WFM-DOAS (Weighting Function Modified DOAS, Buchwitz et al. 2000, 2004, 2005), AMC-DOAS (Air Mass Corrected DOAS, Noël et al. 2004), TOSOMI (Total Ozone retrieval scheme for SCIAMACHY based on the OMI DOAS algorithm, Eskes et al. 2005), SDOAS (Lerot et al. 2009), IMAP-DOAS (Iterative maximum a posteriori DOAS, Frankenberg et al. 2005a, 2005b), IMLM (Iterative Maximum Likelihood Method DOAS, Gloudemans et al. 2008), FSI-WF-DOAS (Full Spectral Initiation Weighting Function Modified DOAS, Barkley et al. 2006) and BIRRA (Better InfraRed Retrieval Algorithm, Schreier et al. 2009). Figure 7-6 illustrates an example of one day of ozone columns derived from nadir observations with one of these schemes, the TOSOMI algorithm. Deriving optically thicker absorbers or line-absorbers based on such DOAS-type methods was successfully demonstrated for O_3, H_2O, O_2, CO, CO_2 and CH_4 (Richter and Wagner 2010).

Parameter	Spectral Window (nm)	Occurrence	Quantity (column)	Retrieval Algorithm	Algorithm Reference
SO_2	315-327	troposphere	total	DOAS	Richter et al. 2006 Lee et al. 2009
				Operational	Lichtenberg et al. 2010
O_3	325-335	troposphere, stratosphere	total	Operational	Lichtenberg et al. 2010
				SDOAS	Lerot et al. 2009
				WFM-DOAS	Weber et al. 2005
				TOSOMI	Eskes et al. 2005
BrO	335-347(51)	troposphere, stratosphere	total, tropospheric, stratospheric	DOAS	Afe et al. 2004
	336-351			Operational	Lichtenberg et al. 2010
HCHO	335(28)-347	troposphere	total	DOAS	Wittrock et al. 2006 De Smedt et al. 2008
OClO	363.5 - 391	stratosphere	total	DOAS	Kühl et al. 2006
	365-389	stratosphere	total	DOAS	Oetjen et al. 2009
				Operational	Lichtenberg et al. 2010
IO	426-440	troposphere	total	DOAS	Saiz-Lopez et al. 2007
	415-430				Schönhardt et al. 2008
NO_2	425-450	troposphere, stratosphere	total, tropospheric, stratospheric	Operational	Lichtenberg et al. 2010
				DOAS	Richter et al. 2005
CHOCHO	435-457	troposphere	total	DOAS	Wittrock et al. 2006 Vrekoussis et al. 2009
H_2O	688-700	troposphere	total	AMC-DOAS	Noël et al. 2004
				operational	Lichtenberg et al. 2010

Table 7-1: Atmospheric geophysical parameters and retrieval algorithms – nadir trace gases in the UV-VIS-NIR.

Parameter	Spectral Window (nm)	Occurrence	Quantity (column)	Retrieval Algorithm	Algorithm Reference
CH_4	1627(30)-1671	troposphere	total	WFM-DOAS	Schneising et al. 2009
				IMAP	Frankenberg et al. 2005a, 2008
CO_2	1558(63)-1594(85)	troposphere	total	WFM-DOAS	Schneising et al. 2008
				IMLM	Houweling et al. 2005
				IMAP	Frankenberg et al. 2005a
				FSI	Barkley et al. 2006
CO	2321(24)-2335	troposphere	total	WFM-DOAS	Buchwitz et al. 2007
				IMLM	Gloudemans et al. 2008, 2009
				IMAP	Frankenberg et al. 2005b
				BIRRA / Operational	Schreier et al. 2009
H_2O	2353-2368	troposphere	total	IMLM	Schrijver et al. 2009
HDO/H_2O ratio	2354.2-2374.2	troposphere	total	IMAP	Frankenberg et al. 2009

Table 7-2: Atmospheric geophysical parameters and retrieval algorithms – nadir trace gases SWIR.

Tables 7-1 and 7-2 summarise the DOAS-type retrieval algorithms as applied to SCIAMACHY data including references.

7.3 Cloud and Aerosol Retrieval

The primary scientific objective of SCIAMACHY is the measurement of atmospheric trace gases in both the troposphere and stratosphere. However, clouds residing in the troposphere interfere with the retrievals from SCIAMACHY measurements mainly by shielding, atmospheric path enhancement, and albedo effects. Similarly, tropospheric and/or stratospheric aerosols impact the trace gas retrieval, as they alter the light path. Therefore, there is a clear need for cloud and aerosol information. In addition, cloud information derived from SCIAMACHY provides relevant data for climate research.

In the UV-VIS and NIR spectral regions the solar radiation is strongly scattered by clouds and aerosols, thereby modifying the Earth reflectance spectrum. The presence of clouds and aerosols and their properties can therefore be determined by analysing the top-of-atmosphere reflection function R, often also termed 'top-of-atmosphere reflectance'. It is defined as

$$R = \pi \frac{I_{dif}}{\mu_0 I_{irr}} \tag{7-11}$$

where μ_0 is the cosine of the solar zenith angle, I_{irr} is the solar irradiance and I_{dif} is the scattered and reflected radiance in the direction towards the satellite sensor.

Prerequisites for high quality information about aerosols and clouds are high spatial resolution and high calibration accuracy of the reflectance measurements. Typical reflectance spectra for various

cloud and surface conditions are shown in Fig. 7-7. Appropriate algorithms are required and available to determine cloud and aerosol properties from SCIAMACHY data. For a summary, the reader is referred to Table 7-3.

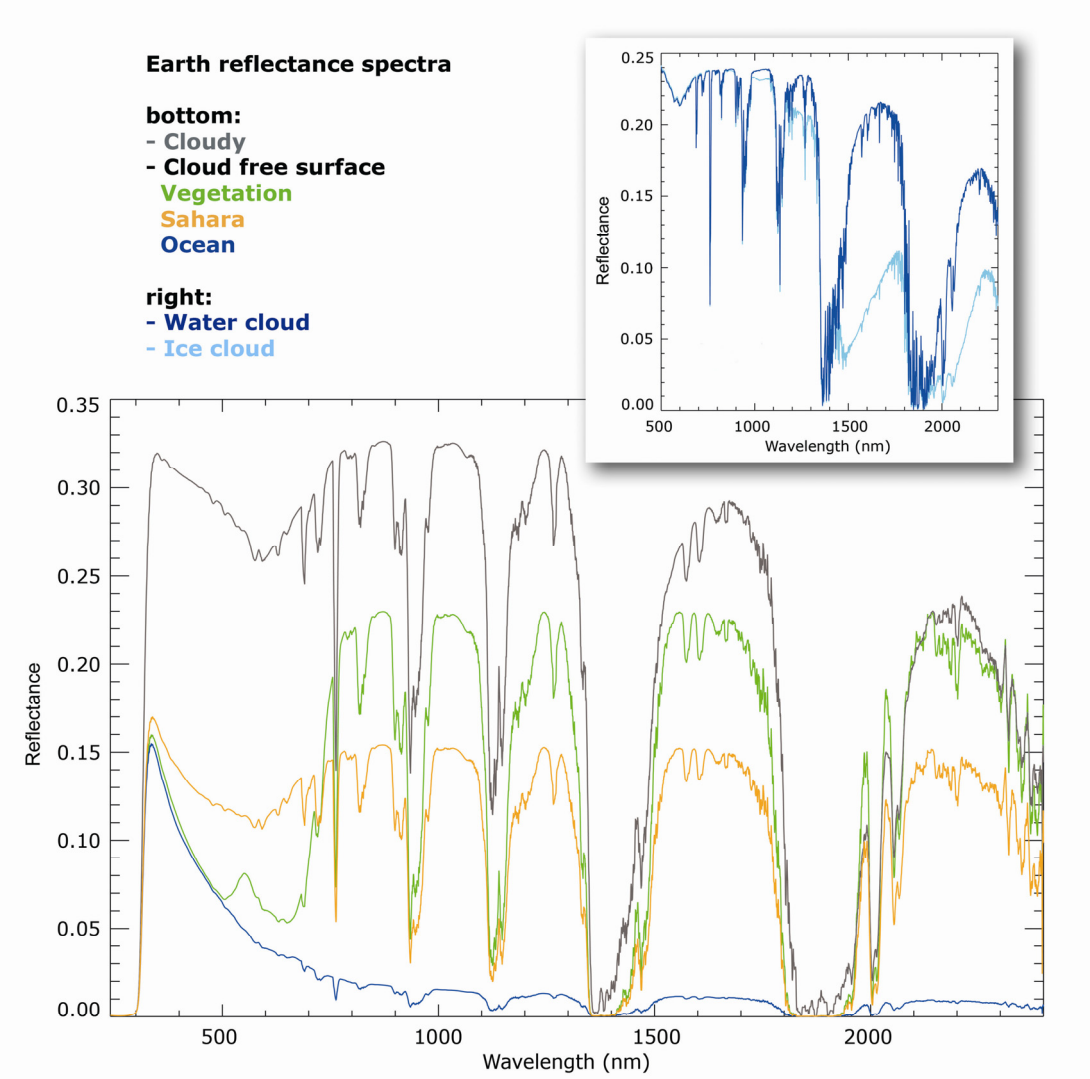

Fig. 7-7: Earth reflectance spectra (Sun normalised intensity) for various cloud and surface conditions. The inset shows the variation in the reflectance spectrum due to changes in the thermodynamic state of water in the cloud from liquid water to ice. The large difference in the reflectance spectrum around 1600 nm for ice and water clouds is used to derive information on the thermodynamical state of water in clouds. (Courtesy: IUP-IFE, University of Bremen)

Cloud Parameters

Information on cloud parameters are of twofold importance in the SCIAMACHY context. Firstly, cloud parameters such as cloud fraction, cloud top pressure (or height) and cloud optical thickness are required to correct the cloud impact on the retrieved trace gas concentrations. Secondly, clouds play an important role in the Earth's climate system. The amount of radiation reflected by the Earth-atmosphere system into outer space depends not only on the cloud cover and the total amount of condensed water in the Earth's atmosphere but also on the size of droplets, the thermodynamic state of water in clouds, and vertical distributions of cloud parameters. The information about microphysical properties and spatial distributions of terrestrial clouds on a global scale can be obtained only with satellite remote sensing systems. Due to their wide spectral range and despite the relatively low spatial resolution, SCIAMACHY data enable the determination of important parameters for climate research like thermodynamic phase or geometrical thickness of clouds.

Cloud Fraction (CF): In order to correct for the effect of clouds, a fast and reliable cloud fraction algorithm is required for SCIAMACHY. Nearly all cloud fraction algorithms for SCIAMACHY use the PMD measurements, as their higher temporal readout frequency translates into a higher spatial resolution as compared to data from channels 1 to 8. The basic principle of the algorithms is that the cloud albedo is much higher (except for ice and snow) than the Earth's surface albedo (see Fig. 7-8). Therefore, a pixel which is contaminated by clouds will generally have a higher detector signal than one that is cloud-free. Cloud fractions can therefore be determined through comparison of PMD intensities. Several derivatives of cloud fraction algorithms using PMD data, such as OCRA (Optical Cloud Recognition Algorithm, Loyola 1998) used in the operational processing, SPCA (SCIAMACHY PMD Cloud Algorithm, Yan 2005) and HICRU (Heidelberg Iterative Cloud Retrieval Utilities, Grzegorski et al. 2004, Grzegorski 2009), are currently being applied to SCIAMACHY data. In addition, algorithms analysing PMD data were developed and applied to discriminate clouds from ice/snow surface, e.g. SPICI (SCIAMACHY PMD Identification of Clouds and Ice/snow, Krijger et al. 2005). Similarly, PMD data can also be used for retrieving further surface classification information (water, sun glint, desert, and vegetation) as demonstrated by SPICS (SCIAMACHY PMD based Identification and Classification of Clouds and Surfaces algorithm, Lotz et al. 2009). The estimation of the cloud fraction and even the distribution of clouds within a SCIAMACHY scene can also be derived from instruments that have a much higher spatial resolution such as MERIS and AATSR on board ENVISAT (Kokhanovsky et al. 2009b, Schlundt et al. 2010).

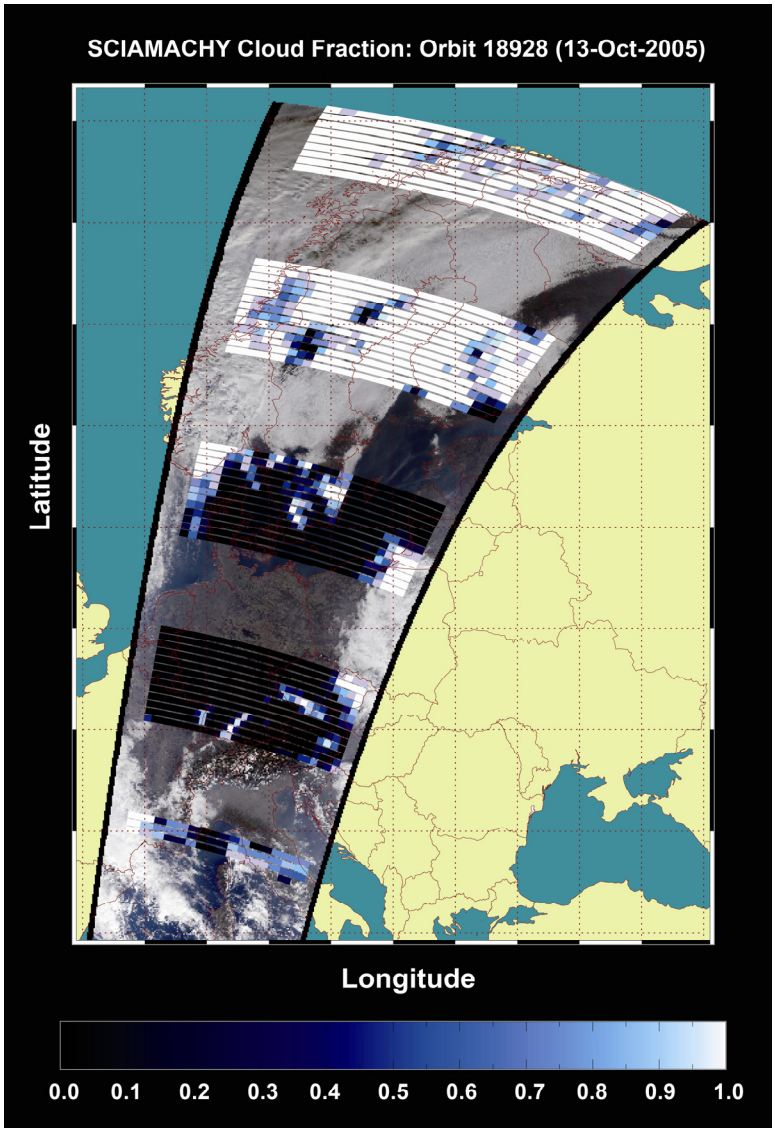

Fig. 7-8: Clouds over Europe on 13 October 2005. Cloud cover as seen in a RGB composite from MERIS with an overlay of the cloud fraction from SCIAMACHY. (Courtesy: C.Schlundt, IUP-IFE)

Cloud Top Height (CTH): CTH can be estimated from the TOA reflection function by using the changes in the penetration depth of solar photons due to strong changes in the absorption of trace gases with known vertical distributions such as O_2 (see Fig. 7-9). The idea for the CTH retrieval from O_2 A-band absorption was originally proposed by Yamomoto and Wark (1961). For SCIAMACHY two algorithms are currently implemented to derive cloud top height from O_2 A-band measurements. These are FRESCO (Fast Retrieval Scheme for Clouds from the Oxygen A-band, Koelemeijer et al. 2001, Fournier et al. 2006) and SACURA (Semi-Analytical Cloud Retrieval Algorithm, Rozanov and Kokhanovsky 2004). FRESCO was recently improved to FRESCO+ by taking into account single Rayleigh scattering (Wang et al. 2008). SACURA delivers not only CTH but also other cloud parameters like cloud phase index, cloud optical thickness and cloud liquid water path for clouds with an optical thickness larger than 5. A corresponding yearly average cloud top height map derived with SACURA for 2004 is shown in Fig. 7-10. It is worth mentioning that in addition to the O_2 A-band, there is also the option to derive CTH information from the O_2-O_2 absorption (Acarreta et al. 2004a), the Ring effect (Joiner et al. 1995, de Beek et al. 2001) or CH_4 absorption (Gloudemans et al. 2009).

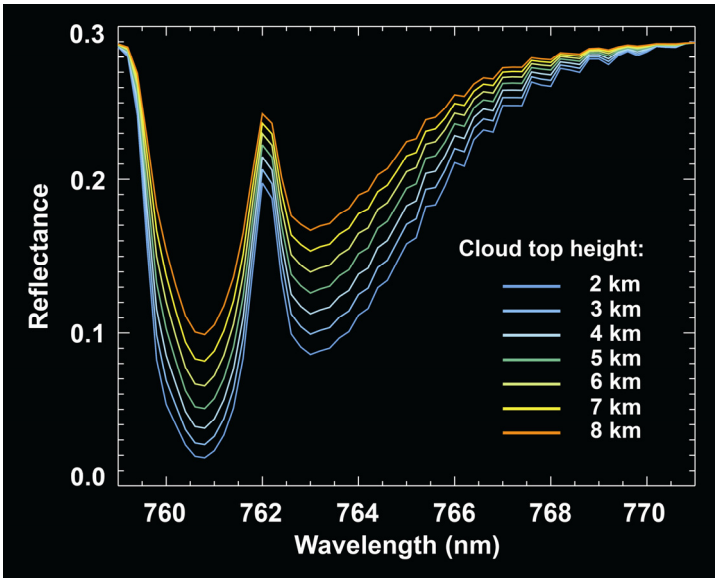

Fig. 7-9: The TOA reflectance in the O_2 A-band as a function of cloud top height. (Courtesy: IUP-IFE, University of Bremen)

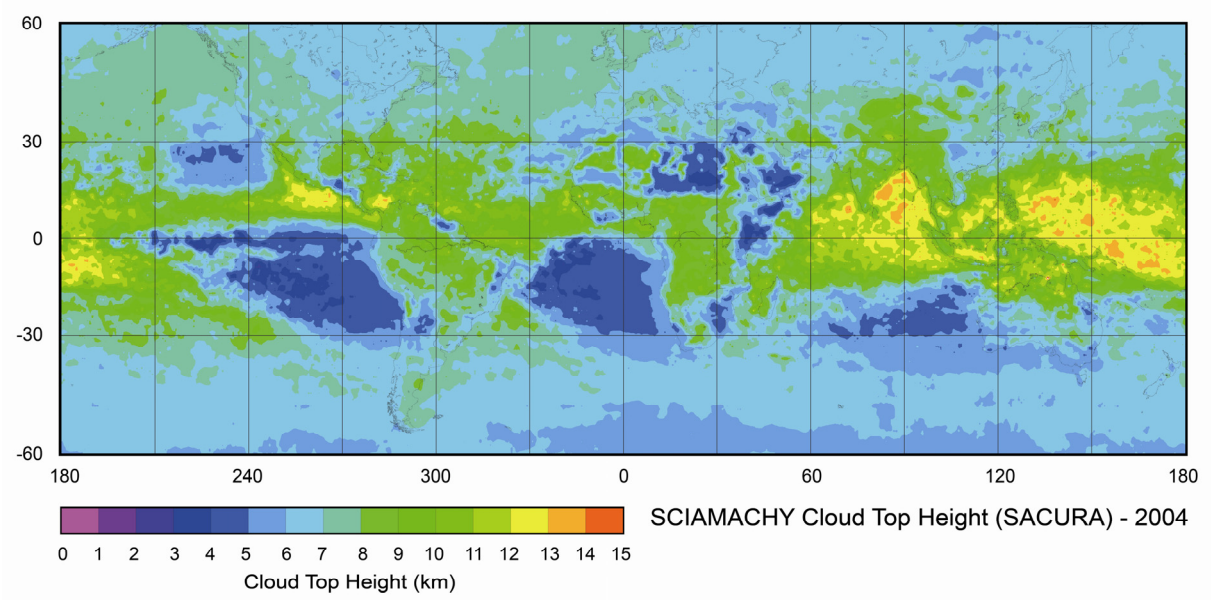

Fig. 7-10: The global distribution of cloud top height as derived with SACURA for 2004. (Courtesy: IUP-IFE, University of Bremen)

Cloud Geometrical Thickness (CGT): O_2 A-band absorption can also be used to obtain an estimate of the CGT (Asano et al. 1995). The CGT values represent an estimate of the light absorption inside a cloud and are therefore well suited for reducing uncertainties in the cloud top altitude measurements. This method was further developed by Kokhanovsky and Rozanov (2005).
Cloud Optical Thickness (COT) and ***Effective Radius ($R_{eff,cld}$)***: Measurements of the Earth reflectance spectrum in the VIS or NIR range outside strong gaseous absorption bands permit derivation of the COT and Effective Radius (Nakajima and King 1990, Platnick et al. 2003). Kokhanovsky et al. (2006a, 2006b) applied the method to SCIAMACHY data. In cases where COT and $R_{eff,cld}$ are known for a liquid water cloud, the liquid water path can be estimated.
Cloud Phase Index (CPI): SWIR reflectance measurements are suitable for obtaining the cloud phase index CPI (Knap et al. 2002, Acarreta et al. 2004b, Kokhanovsky et al. 2007a), as the difference in liquid water and ice absorption around 1.6 μm results in detectable differences in the TOA reflectance (see Fig. 7.7). A discrimination between both is feasible when the reflectance ratio at λ = 1550 nm and 1670 nm is analysed. This can be further extended by simultaneously using thermal IR data from AATSR and SCIAMACHY measurements to detect regions with mixed clouds and clouds containing supercooled water (Kokhanovsky et al. 2007b).

Of the various cloud retrieval algorithms described above, the GOME/SCIAMACHY data processing environment mainly exploits two. One is FRESCO, which uses measurements inside and outside the O_2 A-band (758-778 nm). FRESCO is developed for cloud correction of trace gas retrievals, like O_3 and NO_2. It simultaneously retrieves an effective cloud fraction (CF_{eff}) and an effective cloud top height (CTH_{eff}) assuming that the cloud can be represented as a bright Lambertian surface with a fixed albedo value of 0.8. The second is the combination of OCRA with SACURA. OCRA delivers cloud fraction as input for SACURA to determine CTH and COT. In addition to that, an improved version of SACURA yields cloud geometrical thickness, effective radius, liquid water path, and the cloud thermodynamic state in the case of optically thick clouds (Kokhanovsky et al. 2006a, 2006b).

Tropospheric Aerosol Parameters

Similar to clouds, aerosols play two different roles from SCIAMACHY's perspective. They are both substantial error sources in the retrieval of tropospheric trace gases and provide important geophysical information: aerosol particles affect the radiative budget of the atmosphere directly by absorbing and scattering radiation, and indirectly by influencing cloud properties such as droplet size and hence cloud brightness. Aerosols are characterised by high spatial and temporal variability and can consist of mixtures of chemically and physically different particles, depending on their origin (Pöschl 2005). Typically, they are roughly divided into five categories: (1) sea spray: large particles, no absorption of UV-VIS radiation, (2) mineral dust: large particles, UV-absorbing, (3) biomass burning smoke: small to large particles, strong absorption, (4) volcanic ash: small to large particles, strong absorption, and (5) sulphate droplets: small particles, weak to no absorption. Detection of aerosols by spaceborne instruments makes use of the effect of aerosols on the reflected solar radiation observed at the top of the atmosphere. Contributions from Earth's surface reflections (Fig. 7-7) and atmospheric gases (Fig. 7-3) need to be separated by using available information on the surface properties and the effects of gases in combination with radiative transfer simulations. Thus, the signatures of aerosols can be derived and can be used to retrieve aerosol properties.

Most of the currently existing aerosol retrieval algorithms are aimed at determining the Aerosol Optical Thickness (AOT), i.e. columnar extinction by aerosol particles and its spectral behaviour (Kokhanovsky and de Leeuw 2009a). AOT is extracted by fitting modelled reflectance spectra to the measured reflectance spectra. This approach needs careful constraints based on the knowledge of molecular scattering, absorption and the surface reflectance (von Hoyningen-Huene et al. 2003). Some microphysical parameters, such as aerosol number density and effective particle radius, can be inferred from the magnitude and spectral dependence of the AOT. Other aerosol properties, of which aerosol absorption and layer altitude attract the most interest, need to be derived separately. Although aerosol measurements are not the primary focus of SCIAMACHY, its large wavelength range can be exploited for the study of spectrally dependent aerosol properties in the UV-VIS range and of surface or cloud properties in the near-IR range (von Hoyningen-Huene et al. 2003, 2007). A more standardised and

less complicated way of obtaining information on aerosol properties is offered by application of the UV Aerosol Index (UVAI) algorithm (Herman et al. 1997, Torres et al. 1998, de Graaf and Stammes 2005). The UVAI takes advantage of the strong spectral dependence of molecular Rayleigh scattering in the UV range to obtain semi-quantitative information on aerosol optical thickness, layer altitude, and absorption. The UVAI is most sensitive to elevated layers of aerosols that absorb UV radiation, thus causing a positive UVAI, also widely known as Absorbing Aerosol Index (AAI). The AAI mainly indicates the presence of mineral dust or biomass burning smoke (Fig. 7-11). Initially developed as an error indicator for ozone retrieved from TOMS data (Herman et al. 1997), the AAI is an aerosol quantity with a long data record. The AAI is derived as the positive residual between the measured reflectance from an atmosphere enriched with aerosols and the simulated reflectance of an atmosphere with only Rayleigh scattering, absorption by molecules, plus surface reflection and absorption. Such an algorithm using SCIAMACHY data at 340 nm and 380 nm delivers meaningful AAI values even in the presence of clouds and over bright surfaces (de Graaf and Stammes 2005, de Graaf et al. 2007, as shown in Fig. 7.11). In addition, the concept of the UVAI can also be used for the detection of weakly absorbing ('scattering') aerosols, such as sulphate and secondary organic aerosols, which cause a negative UVAI or Scattering Index (SCI – Penning de Vries et al. 2009). Figure 7-12 shows seasonal averages of the UV Aerosol Index data for July-September 2005 after application of a cloud filter. The colour scale is chosen so that strongly absorbing aerosols, i.e. mineral dust and mainly biomass burning smoke, show up in blue tones, whereas scattering aerosols, such as sulphate and secondary organic aerosols, but also clouds, show up in yellow and red tones. The high positive UVAI values over the global dust belt, defined by the world's largest deserts at around 25°N, indicate large amounts of elevated mineral dust which are transported westward across the Atlantic ocean. High, positive values near the Angolan coast and over the Amazon rainforest are caused by massive biomass burning in the local dry season. Areas influenced by scattering aerosols are not as easily identified. However, when pixels with cloud fractions exceeding 5% were removed from the average, high amounts of scattering aerosols are clearly seen to occur in the South-Eastern US, Eastern China, and in the northern part of South America.

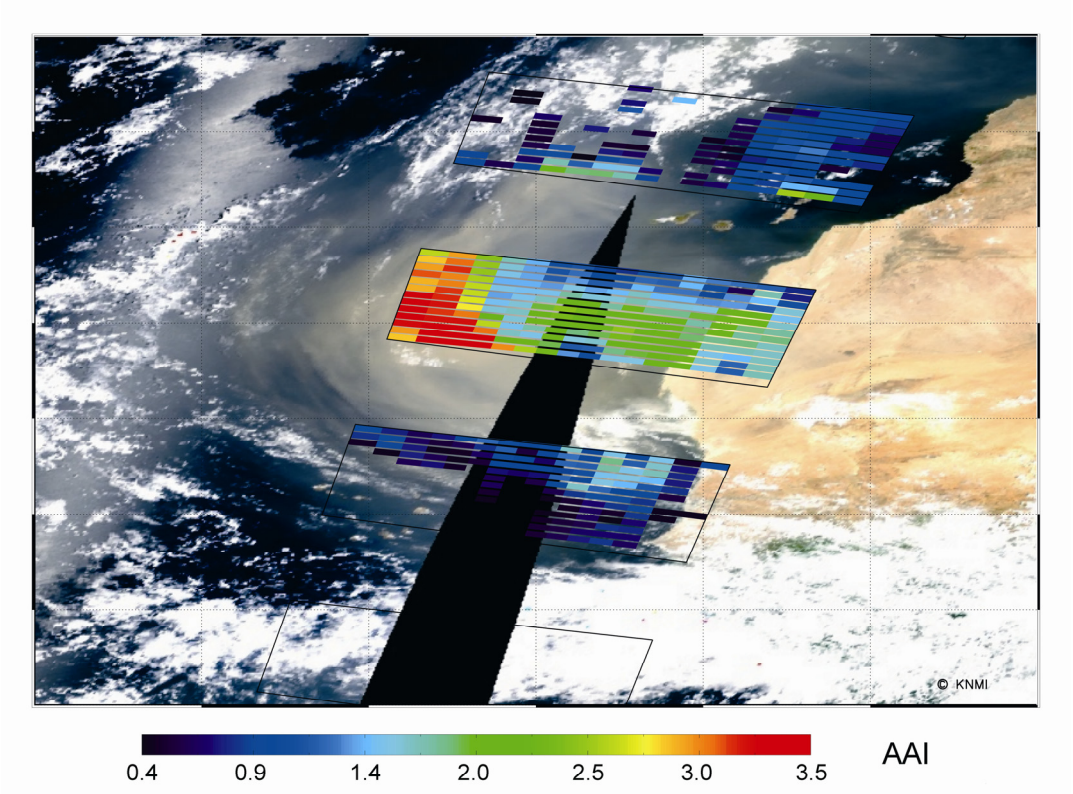

Fig. 7-11: Saharan desert dust outbreak to the Atlantic on 25 July 2004. Shown is the SCIAMACHY AAI at 9:15 UTC of that day overlaid on a MODIS RGB picture, acquired around 11:10 UTC (right side of the plot) and 12:50 UTC (left side of the plot). High SCIAMACHY AAI values coincide with the dust plume, visible as a yellow haze on the MODIS image. (Courtesy: de Graaf et al. 2007)

Parameter	Spectral Window (nm)	Retrieval Algorithm	Algorithm Reference
CF	PMD (RGB)	OCRA	Loyola 1998
		operational	Lichtenberg et al. 2010
		HICRU	Grzegorski et al. 2004
		SPCA	Yan 2005
		SPICI	Krijger et al. 2005
	reflectance near O_2 A-band	FRESCO	Fournier et al. 2006
		SACURA	Kokhanovsky et al. 2006a
	MERIS data	MCFA	Kokhanovsky et al. 2009b
CTH	O_2 A-band	FRESCO	Fournier et al. 2006, Wang et al. 2008
		SACURA / Operational	Kokhanovsky et al. 2006a/b Lichtenberg et al. 2010
	O_2 absorption at ~630	HICRU	Grzegorski 2009
	~477	DOAS	Acarreta et al. 2004a
COT	Reflectance VIS-NIR	SACURA	Kokhanovsky et al. 2006a/b
CGT	O_2 A-band	SACURA	Rozanov and Kokhanovsky 2004
$R_{eff,cld}$	Reflectance VIS-NIR	SACURA	Kokhanovsky et al. 2006a/b
Thermodynamic phase	Reflectance NIR-SWIR	*	Acarreta et al. 2004b
		SACURA	Kokhanovsky et al. 2006b, 2007b
Cloud type	PMD channels	SPICS	Lotz et al. 2009
Cloud - surface discrimination		SPICS	Lotz et al. 2009
AAI	340 and 380	*	de Graaf and Stammes 2005
		operational	Lichtenberg et al. 2010
UVAI	335.5 and 376.5	*	Penning de Vries et al. 2009
AOT	Several wavelengths in the VIS	SCIA-BAER	von Hoyningen-Huene et al. 2003, 2007
	AATSR	SYNAER	Holzer-Popp et al. 2008
Aerosol type	Several wavelengths, combination with AATSR data	SYNAER	Holzer-Popp et al. 2008
Dust altitude	O_2 A-band	*	Kokhanovsky et al. 2010
Phytoplankton groups	340-390, 425-500	PhytoDOAS	Vountas et al. 2007 Bracher et al. 2009
Vegetation	605-685	DOAS	Wagner et al. 2007b
Surface reflectance		*	Grzegorski 2009

Table 7-3: Atmospheric geophysical parameters and retrieval algorithms – nadir cloud, aerosol and surface parameters. Unnamed algorithms are marked by '*'.

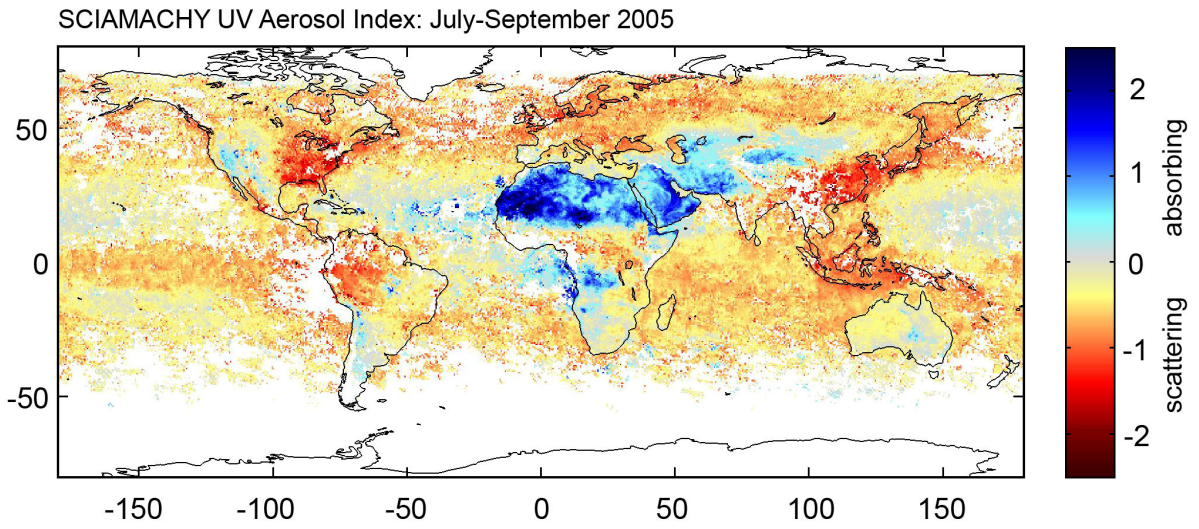

Fig. 7-12: Seasonal average of SCIAMACHY UV Aerosol Index for July-September 2005. Blue indicates absorbing aerosols (mineral dust, biomass burning smoke); red/orange indicate weakly absorbing but scattering aerosols (sulphate and secondary organic aerosols) and remaining clouds. Only pixels with cloud fraction smaller than 5% are included in the average. (Courtesy : M. Penning de Vries, MPI for Chemistry, Mainz)

Further aerosol related retrievals concern the aerosol layer height and the aerosol extinction vertical profile. Both methods use the O_2 A-band (Corradini and Cervino 2006, Kokhanovsky and Rozanov 2010). Finally, even deriving aerosol types is possible by combining SCIAMACHY spectral information with high resolution images from AATSR on ENVISAT. Holzer-Popp et al. (2008) followed this approach by applying the synergistic method SYNAER. A summary of aerosol property retrieving algorithms is given in Table 7-3.

7.4 Surface Parameter Retrieval

The measured earthshine spectra are also affected by surface reflection and absorption, i.e. the broadband ground albedo, and narrowband spectral structures from the surface. Dedicated algorithms were developed to extract surface information from SCIAMACHY data, since the unique spectral coverage in combination with the high spectral resolution offers the possibility to determine new parameters from space. An important prerequisite for the successful application of such algorithms is a good cloud screening (see chapter 7.3) to avoid artefacts introduced by clouds.

Surface Albedo

The spectral surface albedo is an important parameter which determines the sensitivity of satellite observations towards the lower troposphere. It can be derived from TOA reflectance under cloud-free conditions by using a radiative transfer model, as, e.g. pursued by Grzegorski (2009).

Land Vegetation

Light reflected from the Earth's surface towards SCIAMACHY contains the spectral signature of the surface constituents. In case of land, vegetation has a clearly identifiable spectral signature at about 600-680 nm, which can be used to derive vegetation information from measured reflectance spectra (Wagner et al. 2007b). In contrast to existing algorithms which rely on the strong changes of the reflectivity in the red and near infrared spectral region, the new method analyses weak narrowband – only a few nanometers wide – absorption and reflectance structures of vegetation in the abovementioned red spectral range. This method is based on the DOAS approach, which is usually applied for the analysis of atmospheric trace gas concentrations. Since the spectra of atmospheric absorption as well as vegetation absorption and reflectance are simultaneously included in the analysis, the effects of atmospheric absorptions are automatically corrected, in contrast to other

algorithms using hyperspectral data. Another effect of including vegetation spectra is the significant improvement of the results of the trace gas retrievals. Improved sets of vegetation spectra might lead to more accurate and more specific identification of vegetation types in the future.

Oceanic Biological Activity

The DOAS methodology can also be used to derive information about biological activity, i.e. chlorophyll in the ocean. Fitting a modelled Vibrational Raman Scattering (VRS) spectrum of liquid water (Vassilkov et al. 2002) and *in situ* measured phytoplankton absorption reference spectra to optical depths measured by SCIAMACHY permits identifying marine areas with enhanced chlorophyll (Vountas et al. 2007). Phytoplankton absorption reference spectra were obtained during two cruises of the research vessel *Polarstern* (see chapter 9.3). They have been acquired in regions where different species – cyanobacteria and diatoms – dominate the phytoplankton composition. It was demonstrated that the distinct absorption characteristics of the two phytoplankton groups enable their unambiguous identification in SCIAMACHY spectra such that their global surface distribution can be retrieved (Bracher et al. 2009). By combining the phytoplankton absorption with light penetration depth estimated from the inelastic scattering in the liquid water, globally distributed pigment concentrations for both phytoplankton groups can be determined. As in the case of vegetation, accounting for particular spectral signatures from an ocean surface component leads to improved atmospheric trace gas DOAS retrievals over sea.

7.5 Inversion Theory

The forward modelling described in section 7.1 “Radiative Transfer in the Earth’s Atmosphere” is commonly employed to simulate a measured quantity, e.g. intensity of the radiation, for a predefined state of the atmosphere. Contrary to this, the objective of inversion problems is to retrieve certain characteristics of the atmospheric state – for example trace gas concentration profiles – based on the measured quantities. These can be the solar radiance transmitted through the Earth’s atmosphere as observed in the occultation geometry, or the radiance scattered by the Earth’s atmosphere and/or reflected by the surface as observed in the limb or nadir geometry. In this sense, the DOAS method as described above is a special case to solve the inverse problem. Here we will summarise a more general approach to describe the inverse problem and possible solutions. The parameters to be retrieved from the measurements are represented by a *model state vector x*. For example, for trace gas vertical profile retrieval, the model state vector contains the number densities of atmospheric constituents defined at discrete altitude levels. Each state vector can be mapped to the measurement space by means of the forward model operator F to obtain the corresponding measurement vector y, i.e., for each atmospheric state described by vector x, an appropriate measured quantity y can be simulated by using a radiative transfer model (Fig. 7-13).

In the case of SCIAMACHY occultation or limb measurements, the measured quantities are represented by a set of intensities measured at different tangent heights in selected spectral windows; in case of the nadir geometry, the measured quantity is represented by the intensity measured in selected spectral windows. Taking into account that measurements are made to a finite accuracy, a measurement error ε has to be considered which is commonly assumed to be normally distributed with mean zero and known error covariance matrix S_y. Thus, the relationship between the model state vector and the measurement vector can be written as

$$y = F(x) + \varepsilon \tag{7-12}$$

It is interesting to note that the DOAS approach can be derived from (7-12) and is thus only a special case among the methods addressing the inverse problem (see e.g. Rozanov and Rozanov 2010). In order to solve the inverse problem, the generally non-linear relationship in (7-12) can be linearised by expanding the forward model operator, F, as a Taylor series about an initial guess state x_0 (also referenced as *a priori* state) which is the best beforehand estimation of the solution. Ignoring the higher-order terms, one obtains

$$F(x) \approx F(x_0) + \left.\frac{\partial F}{\partial x}\right|_{x_0} (x - x_0) = y_0 + K_0(x - x_0) \tag{7-13}$$

Here, K_0 is the linearised forward model operator. In the discrete representation the linearised forward model operator is given by the weighting function matrix describing the sensitivity of the measured quantities to variations of the atmospheric parameters at different altitude levels. This weighting function matrix is calculated with the radiative transfer model.

Atmospheric inversion problems are usually 'ill-posed', i.e., they do not have a unique solution. Thus, additional constraints need to be introduced to determine a geophysical solution from the set of mathematically allowed solutions and an iterative method has to be used. Most commonly, methods of statistical regularisation, e.g. the *maximum a posteriori* estimate as described by Rodgers (2000), are employed to solve the inversion problem. Using the maximum *a posteriori* estimate, the solution is found by minimising the following quadratic form

$$\left\| (y - y_0) - K_0(x - x_0) \right\|^2_{S_y^{-1}} \quad + \quad \left\| x - x_0 \right\|^2_{S_a^{-1}} \quad \rightarrow \quad \min \tag{7-14}$$

where S_a is the *a priori* covariance matrix of the solution and S_y is the measurement covariance matrix. The latter is usually assumed to be diagonal, i.e. no correlation between measurement errors at different wavelengths or different tangent heights is considered. The linear solution results in

$$x = x_0 + \left(S_a^{-1} + K_0^T S_y^{-1} K_0\right)^{-1} K_0^T S_y^{-1} (y - y_0) \tag{7-15}$$

The non-linearity of the inverse problem can be accounted for by employing the iterative approach as follows:

$$x_{n+1} = x_0 + \left(S_a^{-1} + K_n^T S_y^{-1} K_n\right)^{-1} K_n^T S_y^{-1} \left[(y - y_n) - K_n(x_0 - x_n)\right] \tag{7-16}$$

where subscripts n and $n+1$ denote the number of the iteration.

In the retrieval of the vertical distributions of the atmospheric species, the *a priori* covariance matrix S_a is commonly chosen as a block diagonal matrix, i.e. vertical distributions of different atmospheric trace gases are assumed to be uncorrelated. The diagonal elements of S_a represent the variances of atmospheric trace gases σ which can be derived from, e.g. a climatology.

The quality of the obtained solution is characterised by the *a posteriori* covariance matrix

$$S = \left(K^T S_y^{-1} K + S_a^{-1}\right)^{-1} \tag{7-17}$$

and by the averaging kernels

$$A = \frac{\partial x}{\partial x_{true}} = \left(K^T S_y^{-1} K + S_a^{-1}\right)^{-1} K^T S_y^{-1} K \tag{7-18}$$

characterising the response of the retrieved solution to the variation of the true atmospheric state. The square roots of the diagonal elements of the *a posteriori* covariance matrix are referred to as *theoretical precisions*.

Employing the averaging kernels, the retrieved solution x can be related to the true solution x_{true} as

$$x = x_0 + A(x_{true} - x_0) \tag{7-19}$$

If the model state vector represents a vertical profile of an atmospheric trace gas, the retrieved values at each altitude are expressed as the sum of the *a priori* value at this altitude and of the deviation of the

true profile from the *a priori* profile smoothed with the associated row of the averaging kernel matrix. For an ideal observing system, A is a unit matrix. In reality, the rows of the averaging kernel matrix are peaked with a finite width, which can be regarded as a measure of the vertical resolution of the retrieved profile.

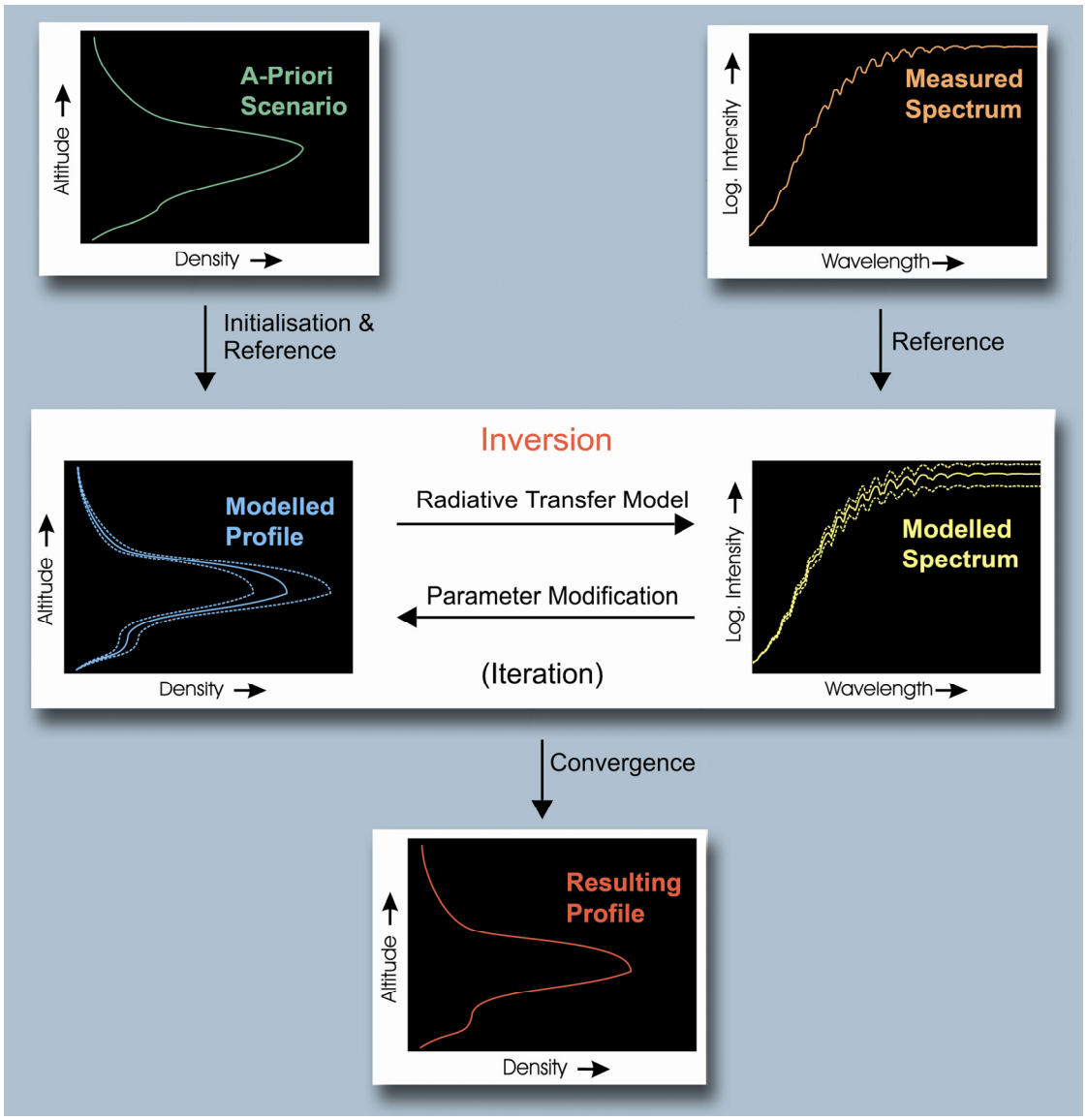

Fig. 7-13: The principle of inversion for the retrieval of geophysical parameters. For further details see the text. (Courtesy: IUP-IFE, University of Bremen)

7.6 Application of Inversion Theory to Limb Retrieval

For the retrieval of the vertical distributions of atmospheric species from the measurements, the so called 'Global Fit' technique is an effective method for inversion. The measurement vector contains the logarithms of the radiances at all selected spectral points and at all line-of-sight angles, both for limb and occultation geometry, referenced to an appropriate extraterrestrial spectrum. In the limb viewing geometry, the extraterrestrial spectrum can be replaced by a limb measurement at an upper tangent height with negligible absorption. Due to this normalisation, the retrieval is relatively robust with respect to the radiometric calibration. In addition, the normalisation significantly reduces the sensitivity of the retrievals with respect to ground albedo and cloud cover. Commonly, before the main inversion step, a preprocessing is performed intended to correct for possible misalignment in the wavelength calibration and to account for known atmospheric corrections such as the Ring effect. If

required, a polynomial can be subtracted from all relevant spectra that account for both missing or inappropriate instrument calibration and unknown scattering properties of the atmosphere.

To illustrate the limb inversion in practice, Fig. 7-14 shows an example of averaging kernels, weighting functions at 338.6 nm, and theoretical precision typical for BrO vertical profile retrievals from SCIAMACHY limb measurements. These results were obtained using the limb measurement at a tangent height of 38.5 km as a reference spectrum. As can be seen, the peak values of the averaging kernels are close to 1.0 only at tangent heights above 15 km. The peak value of about 0.55 at 12 km altitude indicates an increased dependence of the retrieved BrO concentration at this altitude on the BrO concentration at neighbouring altitude levels and the *a priori* information. Looking at the width of the averaging kernels, the height resolution of the measurements can be estimated to be about 3 km, close to the geometrical resolution of the instrument. The weighting functions in the middle panel exhibit relatively sharp peaks near the tangent height down to 18 km tangent height, whereas at all lower tangent heights, the weighting functions peak at about 18 km altitude. Nevertheless, BrO amounts down to 12 km can be retrieved due to the different shapes of the corresponding weighting functions. In accordance with the averaging kernels, the theoretical precision of the BrO vertical profile retrieval shown in the right panel has reasonable values of 10-40% only above 15 km altitude and rapidly decreases below, indicating the low information content in the measurements below 15 km.

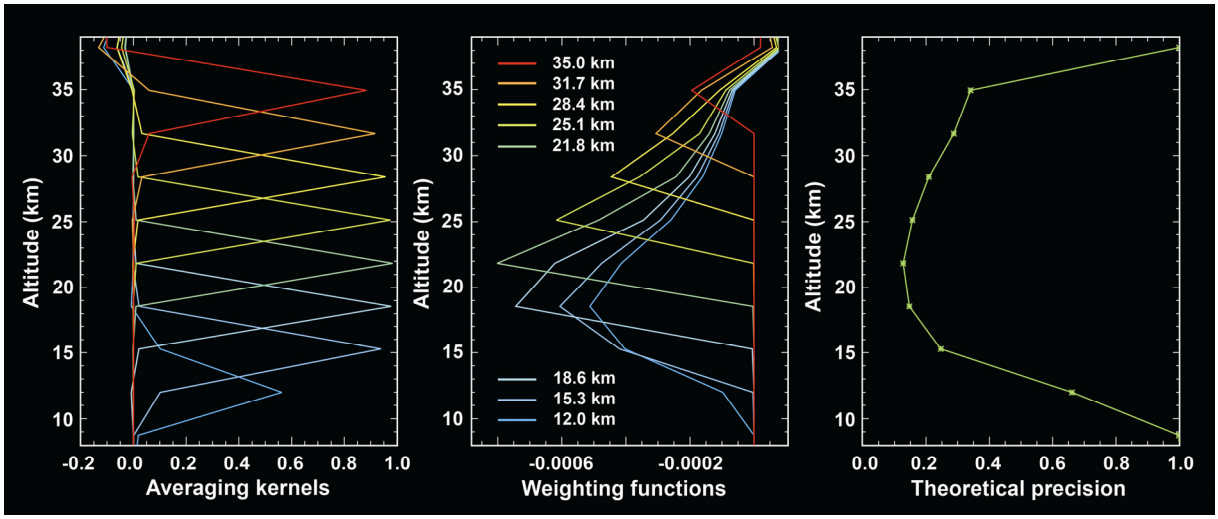

Fig. 7-14: Averaging kernels (left), weighting functions at 338.6 nm (middle), and theoretical precision (right) for BrO vertical profile retrievals from SCIAMACHY limb measurements. (Courtesy: IUP-IFE, University of Bremen)

To date, such types of retrieval algorithms and associated derivates have been used to obtain stratospheric profiles of O_3, NO_2 (Bracher et al. 2005, Rozanov et al. 2005b), BrO (Rozanov et al. 2005b) and H_2O (Rozanov et al. 2010) from SCIAMACHY limb scattering profiles. They were also applied to derive trace gas concentrations from lunar (Amekudzi et al. 2005a, 2005b) and solar (Meyer et al. 2005) occultation measurements. It is worth noting that a similar approach as described above can also be applied to retrieve trace gas information from nadir measurements, as demonstrated for the ozone profile retrieval from GOME nadir measurements (Munro et al. 1998, Hoogen et al. 1999), for example. For a complete list see Table 7-4.

Parameter	Spectral Window (nm)	Occurrence	Quantity	Retrieval Algorithm Reference
O_3	240-310 (selected wavelengths)	mesosphere	profile limb	Rohen et al. 2008
	240-675	stratosphere, mesosphere	profile limb	Sonkaev et al. 2009
	525, 600, 675	stratosphere	profile limb	von Savigny et al. 2005a
	525-590	stratosphere	profile limb	Doicu et al. 2002 Rozanov et al. 2007 Lichtenberg et al. 2010
	520-595	stratosphere	profile sun occultation	Meyer et al. 2005
	510-560	stratosphere	profile moon occultation	Amekudzi et al. 2005a
BrO	338-356	stratosphere	profile limb	Rozanov et al. 2005b Lichtenberg et al. 2010
	338-357			Kühl et al. 2008
	344.1-360			Sioris et al. 2006
OClO	363.5-391	stratosphere	profile limb	Kühl et al. 2008
NO_2	425-450(70)	stratosphere	profile limb	Rozanov et al. 2005b Sioris et al. 2004 Doicu et al. 2002 Lichtenberg et al. 2010
	420-450	stratosphere	profile limb	Kühl et al. 2008
	420-460	stratosphere	profile sun occultation	Meyer et al. 2005
	430-460	stratosphere	profile moon occultation	Amekudzi et al. 2005a
NO_3	610-680	stratosphere	profile moon occultation	Amekudzi et al. 2005b
H_2O	928-968	stratosphere	profile sun occultation	Noël et al. 2010
	1375-1390	lower stratosphere	profile limb	Rozanov et al. 2010
NLC	265-300	mesosphere	indicator, particle radius	von Savigny et al. 2004a
PSC	750, 1090	stratosphere	Indicator	von Savigny et al. 2005b
$T_{mesopause}$	1515-1550	mesosphere	nighttime temperature at mesopause	von Savigny et al. 2004b
Mg, Mg+	1275-290	mesosphere		Scharringhausen et al. 2008

Table 7-4: Atmospheric geophysical parameters and retrieval algorithms – limb and occultation.

All the applications listed above use a continuous spectral range to derive the trace gas information. Another group of limb inversion algorithms employs discrete spectral points in and outside strong trace gas absorption bands for the retrieval of vertical profiles. Retrieval algorithms utilising the difference in absorption between the centre and wings of the ozone Chappuis and Huggins bands were devised by Flittner et al. (2000). In a first step, the limb radiance profiles are normalised with respect to a reference tangent height between 40 and 45 km. For the SCIAMACHY O_3 Chappuis band retrieval (von Savigny et al. 2005a), the normalised limb radiance profiles in the centre of the Chappuis band are divided by the mean of two normalised limb radiance profiles at non-absorbing wavelengths outside the Chappuis band and then analysed in an optimal estimation scheme to retrieve the stratospheric O_3 profiles. Retrievals in the O_3 Chappuis band allow extraction of stratospheric O_3 profiles for altitudes between about 12 km and 40 km. The retrieval range is limited at lower altitudes because the atmosphere becomes optically thick with respect to Rayleigh scattering and/or O_3 absorption. Above about 40 km the O_3 absorption signatures become too weak to be observed. However, normalised limb radiance profiles in the O_3 Hartley and Huggins bands can also be used without further wavelength pairing for the derivation of ozone profiles in the upper stratosphere and lower mesosphere (Rohen et al. 2006). This type of O_3 retrieval was recently extended to cover the lower stratosphere up to the mesosphere (at least 65 km) by combining the absorption in the Hartley and Huggins bands with those in the Chappuis band (Sonkaew et al. 2009). In addition, limb retrievals can derive information about Noctilucent Clouds (NLC), Polar Stratospheric Clouds (PSC) and the temperature at the mesopause ($T_{mesopause}$). References to the algorithms are given in Table 7.4.

A third group of limb inversion algorithms is based on a combination of DOAS and vertical inversion and performed in two steps (Sioris et al. 2004, Sioris et al. 2006, Kühl et al. 2008). In the first step slant column densities, i.e. the integrated concentration of the absorbers along the light path, are derived from the SCIAMACHY limb spectra by DOAS. As a reference spectrum, a measurement at a tangent height is used, where the absorption of the considered trace gas is small. Remaining small abundances of the considered absorbers, which appear at the tangent height of the reference spectrum, are estimated by a latitude-dependent *a-priori* value and are added to the retrieved slant column densities (SCD). In the second step, the trace gas SCD are converted into vertical concentration profiles by applying a radiative transfer model and an inversion scheme like the optimal estimation method (Rodgers 2000) or Chahine-type inversion (Chahine 1970), for example. Just like for nadir DOAS, the limb DOAS retrieval is valid only for weak absorptions and was successfully applied to NO_2, BrO and OClO retrieval (Kühl et al. 2008). Recently, Puķīte et al. (2009) extended the limb DOAS concept to absorbers in an optically thicker atmosphere, thereby improving the retrieval of BrO.

The above mentioned algorithms typically assume that the atmosphere is horizontally homogeneous, which is not fulfilled under all conditions. For example, substantial gradients exist across the Arctic polar vortex boundary. Puķīte et al. (2010) investigated the effect of horizontally inhomogeneous distributions of trace gases along the flight/viewing direction on the retrieval of profiles. They introduced a method called 'limb 2D tomography' to correct for this effect by combining consecutive limb scanning sequences and using the overlap in their measurement sensitivity regions. The retrieval was applied to synthetic as well as to real SCIAMACHY data (Fig. 7-15). It was found that, if horizontal inhomogeneity is not properly accounted for, typical errors of 20% for NO_2 and up to 50% for OClO around the altitude of the profile peak can arise for measurements close to the Arctic polar vortex boundary in boreal winter.

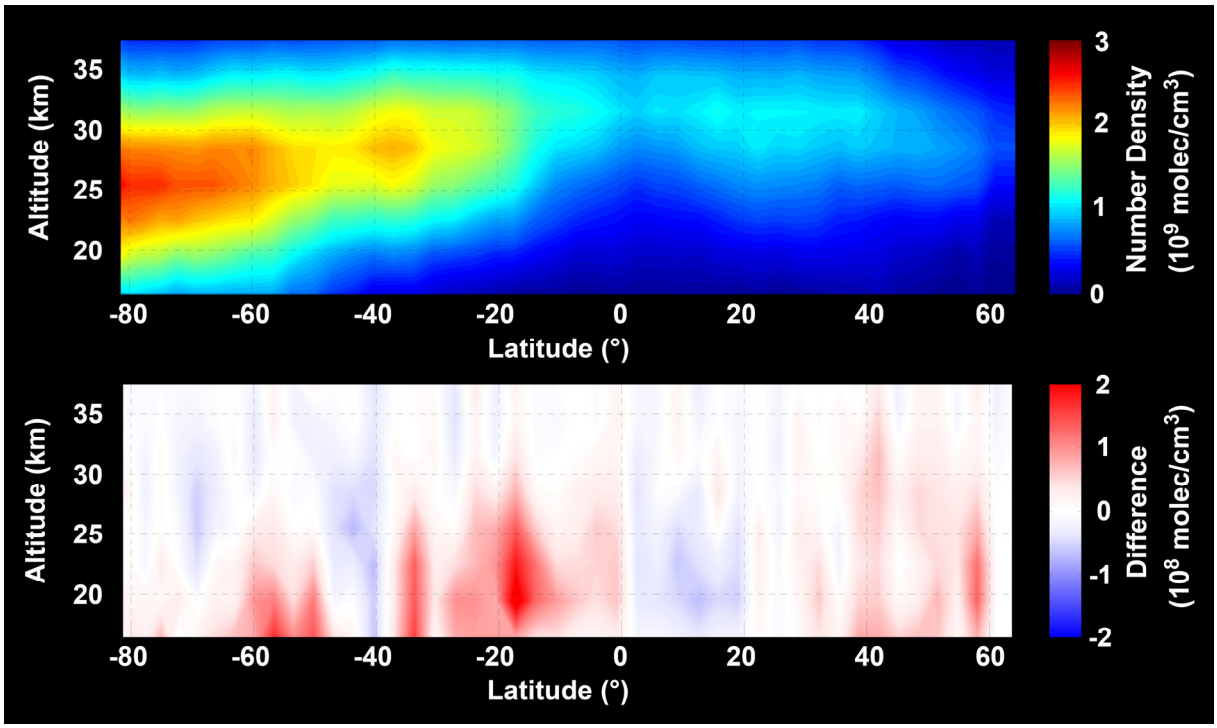

Fig. 7-15: NO_2 densities (top panel) as derived from SCIAMACHY limb measurements using the limb 2D tomography method for the orbit 35499 (14 December 2008) consisting of limb states only. In the bottom panel, the difference to results from the less accurate 1D approach is illustrated. (Courtesy: J. Puķīte, MPI for Chemistry, Mainz)

To derive meteoric metal content at different levels of the atmosphere from limb and nadir measurements, Scharringhausen et al. (2008) developed and applied a limb-nadir 2D tomographic retrieval scheme based on optimal estimation to evaluate SCIAMACHY limb and nadir emissions simultaneously for every SCIAMACHY orbit. The inversion algorithm gives the total content as well as partial columns in the thermosphere and in the mesosphere. This retrieval successfully distinguished the mesospheric from the thermospheric column abundances of MgII and MgI for the first time.

The wide variety of retrieval algorithms currently applied to SCIAMACHY limb and occultation data are summarised in Table 7-4, together with their corresponding references.

7.7 Derivation of Tropospheric Information

Distributions of trace gases in the troposphere are of prime scientific, as well as public interest. Two cases need to be distinguished:

- Constituents with the majority of the atmospheric amount residing in the lower troposphere (e.g. CO, CH_4, CO_2, HCHO, SO_2, H_2O): The total column derived from UV-VIS and SWIR solar backscatter measurements with the techniques described in chapter 7.2 directly represents the tropospheric column amount including the boundary layer under cloud-free conditions.
- Trace gases with comparable column amounts in the troposphere and stratosphere (e.g. BrO, NO_2) or with the stratospheric amount dominating the total column (e.g. O_3).

For the latter case, dedicated techniques are required to separate the tropospheric and the stratospheric contributions. One approach is to use measurements over a clean-air region as a background, the so-called 'Reference Sector Method' (see below). In addition, SCIAMACHY's unique limb/nadir matching capabilities (see chapter 4) provide a nearly simultaneous stratospheric profile measurement for each nadir measurement. In that respect, SCIAMACHY is clearly superior to GOME on ERS-2, which obtained measurements of the same species in the UV-VIS range but only in nadir geometry.

An error analysis for approaches to derive tropospheric NO_2, which provides error components and retrieval uncertainties, has been given by Boersma et al. (2004).

Reference Sector Method

The Reference Sector Method (RSM), also referred to as *Tropospheric Residual Method* (Velders et al. 2001, Richter and Burrows 2002, Martin et al. 2002), allows the separation of tropospheric and stratospheric contributions to the total NO_2 content under the assumption of negligible tropospheric NO_2 concentrations over the clean, free Pacific Ocean. It is assumed that the stratospheric NO_2 distribution is homogeneous with longitude. Then the tropospheric NO_2 is primarily the difference between the total column measured over a polluted area and the total column measured over the clean Pacific Ocean. This technique needs no stratospheric profile information and can therefore be applied to generate a consistent GOME – SCIAMACHY tropospheric NO_2 data set (see chapter 10). A similar idea is also pursued in the retrieval of tropospheric HCHO and SO_2 concentrations to correct for artificial biases.

Limb/Nadir Matching

Especially for regions with low or moderate pollution levels, the errors in the retrieved tropospheric columns introduced by the simple Reference Sector Method can become important. To reduce the error, it is required to use the measured stratospheric column above the ground scene of interest. SCIAMACHY with its limb/nadir matching measurement mode provides radiances from the same volume of air in limb and nadir geometry. This allows inference of vertical stratospheric concentration profiles directly over the region of the nadir measurement. Integrating these profiles from the tropopause upwards yields the measured stratospheric column above the target area while the co-located nadir measurement provides the total column amount. In short, tropospheric column is then determined as the difference between the total and the stratospheric column. An initial application of this approach to derive tropospheric ozone and NO_2 was presented in Sierk et al. (2006) and Sioris et al. (2004). The method described here is unique in the sense that the information on the stratospheric content is taken directly from the co-located limb measurement and no other assumptions (longitudinal homogeneity) nor an estimate of the stratospheric column from a model or from data assimilation are necessary.

Further progress was recently made by Beirle et al. (2010) when the potential and the limitations of SCIAMACHY limb measurements for estimating stratospheric column densities of NO_2 in comparison to a simple RSM were investigated. The direct, Absolute Limb Correction (ALC) scheme calculates stratospheric limb vertical column densities (VCD) by integrating the profiles from 15 km to 42 km. These improve spatial patterns of tropospheric NO_2 column densities at high latitudes compared to the simple RSM. However, it can result in artificial zonal stripes at low latitudes. Thus, an additional limb correction method was defined, which turned out to successfully reduce stratospheric artefacts in the resulting tropospheric data product without introducing new ones (Fig. 7-16). It applies the same reference sector correction both to the nadir and limb VCD. This new stratospheric estimation scheme, the Relative Limb Correction (RLC), improves monthly mean tropospheric slant column densities significantly, e.g. from a bias of -1×10^{15} molec/cm^2 (using a simple RSM) to nearly zero in the Atlantic ocean, and from $+1\times10^{15}$ molec/cm^2 to nearly zero over Siberia, at 50°N in January.

Data Assimilation – the NO_2 Example

Data assimilation (see chapter 8.4) provides another possibility for the separation of tropospheric and stratospheric contributions. NO_2 permanently resides in the stratosphere and shows significant amounts in the troposphere near source areas. Firstly, the stratospheric and tropospheric parts of the column need to be separated and subsequently, a tropospheric airmass factor has to be applied to the tropospheric slant column. At KNMI, in collaboration with BIRA-IASB, a data assimilation system was applied to NO_2 to derive the stratospheric part of the slant column by assimilation of observed slant columns in a chemistry-transport model (Eskes et al. 2003). This resulted in a stratospheric analysis consistent with the observations and with the variations observed in the stratosphere that are

due to atmospheric dynamics and chemical reactions. The tropospheric NO_2 slant column was then extracted by subtracting the assimilated stratospheric slant column from the retrieved total slant column.

In a similar way the stratospheric NO_2 slant column density, exactly for the SCIAMACHY overpass time, was derived from the stratospheric chemistry transport model ROSE at DLR-DFD. To avoid a bias, the modelled stratospheric slant columns were scaled to 'clean conditions' over the Pacific Ocean. The tropospheric NO_2 slant column was then again extracted by subtracting the modelled stratospheric slant column from the retrieved total slant column. Fig. 7-17 shows the resulting tropospheric NO_2 distribution over Europe. The tropospheric NO_2 distributions could be further improved by using NO_2 profile shapes estimated with air quality models like EURAD. In this case, properties of clouds, aerosols and the surface also need to be taken into account.

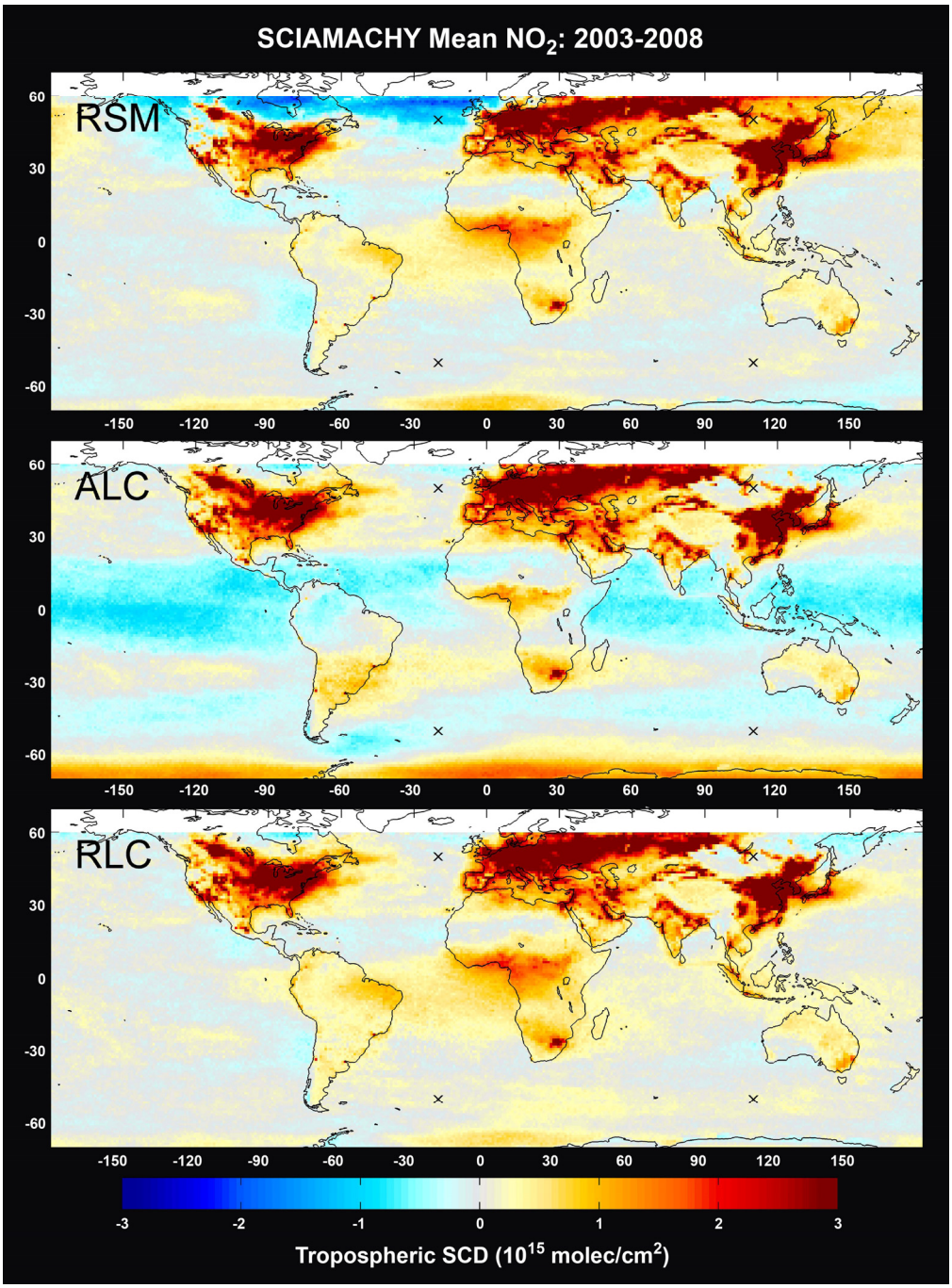

Fig. 7-16: Mean tropospheric NO_2 slant column densities as derived for the period 2003-2008 using the Reference Sector Method (RSM – top), Absolute Limb Correction (ALC – middle) and Relative Limb Correction (RLC – bottom). (Courtesy: S. Beirle, MPI for Chemistry, Mainz)

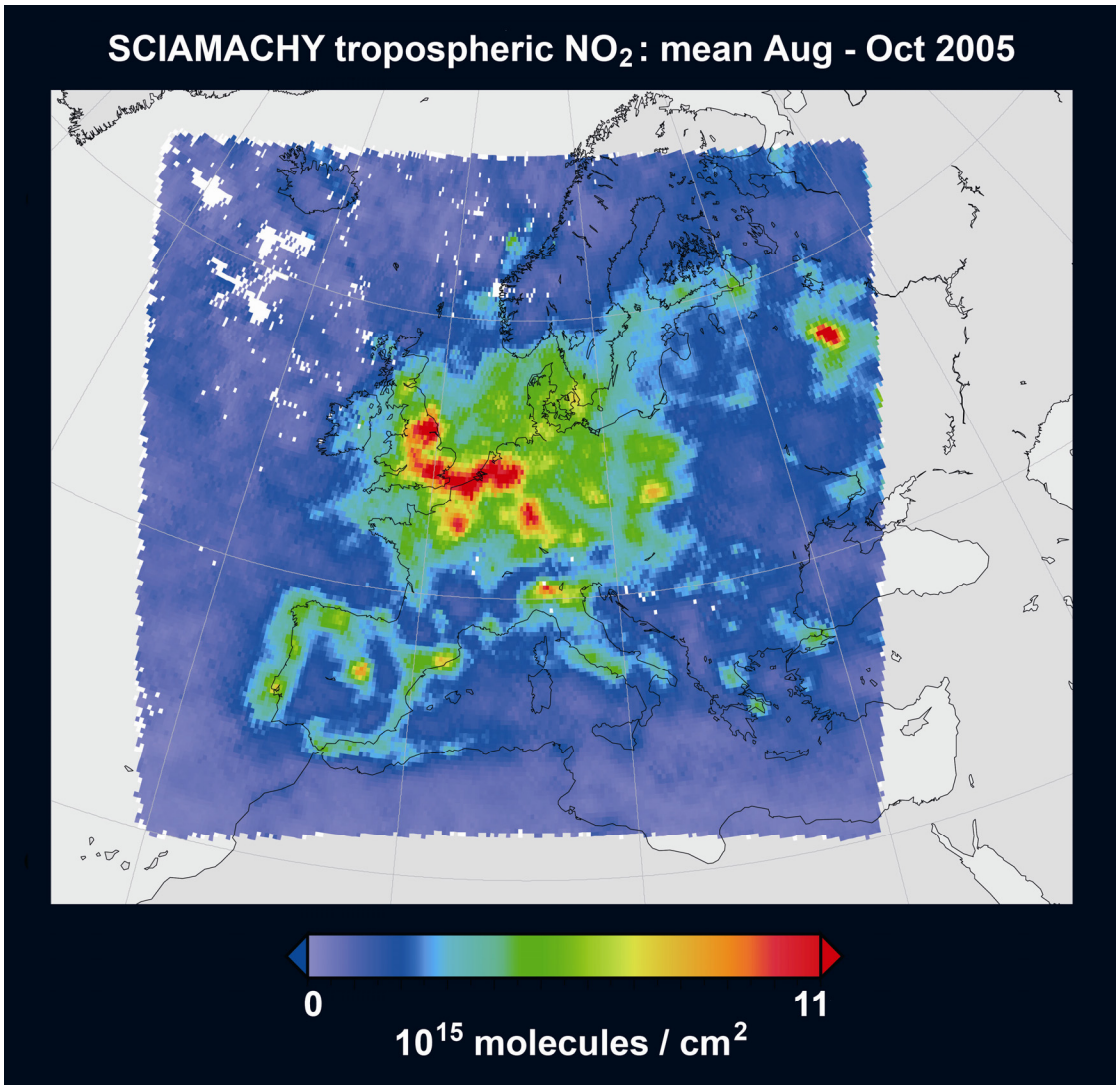

Fig. 7-17: Mean tropospheric NO_2 vertical column densities over Europe as derived from SCIAMACHY for August to October 2005 with the DLR-DFD assimilation approach. (Courtesy: T. Erbertseder, DLR-DFD)

References

Acarreta, J.R, de Haan, J.F. and Stammes, P. 2004a. Cloud pressure retrieval using $O_2 – O_2$ absorption band at 477 nm. *J. Geophys. Res.*, 109, D05204, doi:10.1029/2003JD003915.

Acarreta, J.R., Stammes, P. and Knap, W.H. 2004b. First retrieval of cloud phase from SCIAMACHY spectra around 1.6 micron. *Atmos. Res.*, 72, 89-105.

Afe, O.T., Richter, A., Sierk, B., Wittrock, F., and Burrows, J.P. 2004. BrO emission from volcanoes: A survey using GOME and SCIAMACHY measurements. *Geophys. Res. Lett.*, 31, L24113, doi:10.1029/2004GL020994.

Amekudzi, L.K., Bracher, A., Meyer, J., Rozanov, A., Bovensmann, H., Burrows, J.P. 2005a. Lunar occultation with SCIAMACHY: First retrieval results. *Adv. Space Res.*, 36, 906-914.

Amekudzi, L.K., Sinnhuber, B.-M., Sheode, N.V., Meyer, J., Rozanov, A., Lamsal, L., Bovensmann, H. and Burrows, J.P. 2005b. Retrieval of stratospheric NO_3 vertical profiles from SCIAMACHY lunar occultation measurement over the Antarctic. *J. Geophys. Res.*, 110, D20304, doi:10.1029/2004JD005748.

Asano, S., Shiobara, M. and Uchiyama, A. 1995. Estimation of cloud physical parameters from airborne solar spectral reflectance measurements for stratocumulus clouds. *J. Atmos. Sci.*, 52, 3556-3576.

Barkley, M.P., Frieß, U. and Monks, P.S. 2006. Measuring atmospheric CO_2 from space using Full Spectral Initiation (FSI) WFM-DOAS. *Atmos. Chem. Phys.*, 6, 3517-3534.

Bates, D.R. 1984. Rayleigh scattering by air. *Planet Space Sci*., 32, 785-790.

Beirle, S., Kühl, S., Pukite, J., and Wagner, T. 2010. Retrieval of tropospheric column densities of NO_2 from combined SCIAMACHY nadir/limb measurements. *Atmos. Meas. Tech.*, 3, 283-299.

Boersma, K.F., Eskes, H.J. and Brinksma, E.J. 2004. Error analysis for tropospheric NO_2 retrieval from space. *J. Geophys. Res.*, 109, D04311, doi:10.1029/2003JD003962.

Bracher, A., Sinnhuber, M., Rozanov, A. and Burrows, J.P. 2005. NO_2 Modelling used for the comparison of NO_2 Satellite Measurements at different Solar Zenigh Angles. *Atmos. Chem. Phys.*, 4, 5515-5548.

Bracher, A., Vountas, M., Dinter, T., Burrows, J.P., Röttgers, R., and Peeken, I. 2009. Cyanobacteria and diatoms from space using PhytoDOAS on SCIAMACHY data. *Biogeosciences*, 6, 751-764.

Buchwitz, M., Rozanov, V.V. and Burrows, J.P. 2000. A near-infrared optimized DOAS method for the fast global retrieval of atmospheric CH_4, CO, CO_2, H_2O, and N_2O total column amounts from SCIAMACHY Envisat-1 nadir radiances. *J. Geophys. Res.*, 105, 15231-15245.

Buchwitz, M., de Beek, R., Bramstedt, K., Noël, S., Bovensmann, H. and Burrows, J.P. 2004. Global carbon monoxide as retrieved from SCIAMACHY by WFM-DOAS. *Atmos. Chem. Phys.*, 4, 1954-1960.

Buchwitz, M., de Beek, R., Burrows, J.P., Bovensmann, H., Warneke, T., Notholt, J., Meirink, J.F., Goede, A.P.H., Bergamaschi, P., Körner, S., Heimann, M. and Schulz. A. 2005. Atmospheric methane and carbon dioxide from SCIAMACHY satellite data: Initial comparison with chemistry and transport models. *Atmos. Chem. Phys.*, 5, 941-962.

Buchwitz, M., Khlystova, I., Bovensmann, H., and Burrows, J.P. 2007. Three years of global carbon monoxide from SCIAMACHY: comparison with MOPITT and first results related to the detection of enhanced CO over cities. *Atmos. Chem. Phys.*, 7, 2399-2411.

Burrows, J.P., Weber, M., Buchwitz, M., Rozanov, V., Ladstätter-Weißenmayer, A., Richter, A., DeBeek, R., Hoogen, R., Bramstedt, K., Eichmann, K.-U., Eisinger, M. and Perner, D. 1999. The Global Ozone Monitoring Experiment (GOME): Mission Concept and First Scientific Results. *J. Atmos. Sci.,* 56, 151-175.

Chance, K., Spurr, R.J.D. 1997. Ring effect studies: Rayleigh scattering, including molecular parameters for rotational Raman scattering, and the Fraunhofer spectrum. *Appl. Opt*., 36, 5224-5230.

Chance, K. 1998. Analysis of BrO measurements from the Global Ozone Monitoring Experiment. *Geophys. Res. Lett.*, 25, 3335-8.

Chance, K., Kurosu, T.P. and Sioris, C.E. 2005. Undersampling correction for array-detector based satellite spectrometers. *Appl. Opt.*, 44, 1296-1304.

Chahine, M.T. 1970. Inverse problems in radiative transfer: Determination of atmospheric parameters. *J. Atm. Sci.*, 27, 960967.

Corradini, S. and Cervino, M. 2006. Aerosol extinction coefficient profile retrieval in the oxygen A-band considering multiple scattering atmosphere. Test case: SCIAMACHY nadir simulated measurements. *J. Quant. Spectr. and Rad. Transfer*, 97, 354-380.

de Beek, R., Vountas, M., Rozanov, V.V., Richter, A. and Burrows, J.P. 2001. The Ring effect in the cloudy atmosphere. *Geophys. Res. Lett.*, 28, 721-724.

de Graaf, M. and Stammes, P. 2005. SCIAMACHY Absorbing Aerosol Index – calibration issues and global results from 2002-2004. *Atmos. Chem. Phys.*, 5, 2385-2394.

de Graaf, M., Stammes, P., Aben, E.A.A. 2007. Analysis of reflectance spectra of UV-absorbing aerosol scenes measured by SCIAMACHY. *J. Geophys. Res.*, 112, D02206, doi:10.1029/2006JD007249.

De Smedt, I., Müller, J.-F., Stavrakou, T., van der A, R., Eskes, H. and Van Roozendael, M. 2008. Twelve years of global observations of formaldehyde in the troposphere using GOME and SCIAMACHY sensors. *Atmos. Chem. Phys.*, 8, 4947-4963.

Deutschmann, T., Beirle, S., Frieß, U., Grzegorski, M., Kern, C., Kritten, L., Platt, U., Puķīte, J., Wagner, T., Werner, B., Pfeilsticker, K. 2010. The Monte Carlo Atmospheric Radiative Transfer Model McArtim: Introduction and Validation of Jacobians and 3D Features, accpeted for publication in *J. Quant. Spectr. Rad. Transf.*.

Doicu, A., Schreier, F. and Hess, M. 2002. Iteratively regularized Gauss-Newton method for atmospheric remote sensing. *Comp. Phys. Comm.*, 148, 214-226.

Dorf, M., Bösch, H., Butz, A., Camy-Peyret, C., Chipperfield, M.P., Engel, A., Goutail, F., Grunow, K., Hendrick, F., Hrechanyy, S., Naujokat, B., Pommereau, J.-P., Van Roozendael, M., Sioris, C., Stroh, F., Weidner, F. and Pfeilsticker, K. 2006. Balloon-borne stratospheric BrO measurements: comparison with Envisat/SCIAMACHY BrO limb profiles. *Atmos. Chem. Phys.*, 6, 2483-2501.

Eskes, H. J., van Velthoven, P.F.J., Valks, P.J.M. and Kelder, H.M. 2003. Assimilation of GOME total ozone satellite observations in a three-dimensional tracer transport model. *Quart. J. Roy. Meteorol. Soc.*, 129, 1663-1681.

Eskes, H.J., van der A, R.J., Brinksma, E.J., Veefkind, J.P., de Haan, J.F. and Valks, P.J.M. 2005. Retrieval and validation of ozone columns derived from measurements of SCIAMACHY on Envisat. *Atmos. Chem. Phys. Discuss.*, 5, 4429-4475.

Flittner, D.E., Bhartia, P.K. and Herman, B.M. 2000. O_3 profiles retrieved from limb scatter measurements: Theory. *Geophys. Res. Lett.*, 27, 2061-2064.

Fournier, N., Stammes, P., de Graaf, M., van der A, R., Piters, A., Grzegorski, M. and Kokhanovsky, A. 2006. Improving cloud information over deserts from SCIAMACHY Oxygen A-band measurements. *Atmos. Chem. Phys.*, 6, 163-172.

Frankenberg, C., Platt, U. and Wagner, T. 2005a. Iterative maximum a posteriori (IMAP)-DOAS for retrieval of strongly absorbing trace gases: Model studies for CH_4 and CO_2 retrieval from near infrared spectra of SCIAMACHY onboard ENVISAT. *Atmos. Chem. Phys.*, 5, 9-22.

Frankenberg, C., Platt, U. and Wagner, T. 2005b. Retrieval of CO from SCIAMACHY onboard ENVISAT: detection of strongly polluted areas and seasonal patterns in global CO abundances. *Atmos. Chem. Phys.*, 5, 1639-1644.

Frankenberg, C. Bergamaschi, P., Butz, A., Houweling, S., Meirink, J.F., Notholt, J., Petersen, A.K., Schrijver, H., Warneke, T., and Aben, I. 2008. Tropical methane emissions: A revised view from SCIAMACHY onboard ENVISAT. *Geophys. Res. Letters*, 35, L15811, doi:10.1029/2008GL034300.

Frankenberg, C., Yoshimura, K., Warneke, T., Aben, I., Butz, A., Deutscher, N., Griffith, D., Hase, F., Notholt, J., Schneider, M., Schrijver, H. and Röckmann, T. 2009. Dynamic Processes Governing Lower-Tropospheric HDO/H2O Ratios as Observed from Space and Ground. *Science*, 325, 1374.

Gloudemans, A.M.S., Schrijver, H., Hasekamp, O.P. and Aben, I. 2008. Error analysis for CO and CH_4 total columns retrieved from SCIAMACHY 2.3 μm spectra. *Atmos. Chem. Phys.*, 8, 3999-4017.

Gloudemans, A.M.S., de Laat, A.T.J., Schrijver, H., Aben, I., Meirink, J.F. and van der Werf, G.R. 2009. SCIAMACHY CO over land and oceans: 2003-2007 interannual variability. *Atmos. Chem. Phys.*, 9, 3799-3813.

Grainger, J.F. and Ring, J. 1962. Anomalous Fraunhofer line profiles. *Nature,* 193, 762-762.

Grzegorski, M., Frankenberg, C., Platt, U., Wenig, M., Fournier, N., Stammes, P. and Wagner, T. 2004. Determination of cloud parameters from SCIAMACHY data for the correction of tropospheric trace gases. *Proc. ENVISAT & ERS Symposium*, Salzburg, Austria, ESA SP-572.

Grzegorski, M. 2009. Cloud retrieval from UV/VIS satellite instruments (SCIAMACHY and GOME). *Ph.D. thesis*, University of Heidelberg.

Herman, J.R., Bhartia, P.K., Torres, O., Hsu, C., Seftor, C. and Celarier, E.A. 1997. Global distributions of UV-absorbing aerosols from NIMBUS 7/TOMS data. *J. Geophys. Res.*, 102, 16911-16922.

Holzer-Popp, T., Schroedter-Homscheidt, M., Breitkreuz, H., Martynenko, D. and Klüser, L. 2008. Improvements of synergetic aerosol retrieval for ENVISAT. *Atmos. Chem. Phys.*, 8, 7651-7672.

Hoogen, R., Rozanov, V.V. and Burrows, J.P. 1999. Ozone profiles from GOME satellite data: algorithm description and first validation. *J. Geophys. Res.*, 104, 8263-8280.

Houweling, S., Hartmann, W., Aben, I., Schrijver, H., Skidmore, J., Roelofs, G.-J. and Breon, F.-M. 2005. Evidence of systematic errors in SCIAMACHY-observed CO_2 due to aerosols. *Atmos. Chem. Phys.*, 5, 3003-3013.

Joiner, J., Bhartia, P.K., Cebula, R.P., Hilsenrath, E., McPeters, R.D. and Park, H. 1995. Rotational Raman scattering (Ring effect) in satellite backscatter ultraviolet measurements. *Appl. Opt.*, 34, 4513-4525.

Kaiser, J.W. and Burrows, J.P. 2003. Fast weighting functions for retrievals from limb scattering measurements. *J. Quant. Spectr. Rad. Transfer*, 77, 273-283.

Knap, W.H, Stammes, P. and Koelemeijer, R.B.A. 2002. Cloud thermodynamic phase determination from near-infrared spectra of reflected sunlight. *J. Atmos. Sci*., 59, 83-96.

Koelemeijer, R.B.A., Stammes, P., Hovenier, J.W. and de Haan, J.F. 2001. A fast method for retrieval of cloud parameters using oxygen A band measurements from the Global Ozone Monitoring Experiment. *J. Geophys. Res.*, 106, 3475-3490.

Kokhanovsky, A.A. and Rozanov, V.V. 2005. Cloud bottom altitude determination from a satellite. *IEEE Transactions on Geoscience and Remote Sensing Letters*, 2, 280-283.

Kokhanovsky, A.A., Rozanov, V.V., Nauss, T., Reudenbach, C., Daniel, J.S., Miller, H.L. and Burrows, J.P. 2006a. The semianalytical cloud retrieval algorithm for SCIAMACHY: I. Validation. *Atmos. Chem. Phys.*, 6, 1905-1911.

Kokhanovsky, A.A., von Hoyningen-Huene, W., Rozanov, V.V., Noël, S., Gerilowski, K., Bovensmann, H., Bramstedt, K., Buchwitz, M. and Burrows, J.P. 2006b. The semianalytical cloud retrieval algorithm for SCIAMACHY II. The application to MERIS and SCIAMACHY data. *Atmos. Chem. Phys.*, 6, 4129-4136.

Kokhanovsky, A.A., Vountas, M., Rozanov, V.V., Lotz, W., Bovensmann, H. and Burrows, J.P. 2007a, Global cloud top height and thermodynamic phase distribution as obtained by SCIAMACHY on ENVISAT. *Int. J. Remote Sensing*, 28, 4499-4507.

Kokhanovsky, A.A., Jourdan, O., Burrows, J.P. 2007b. The cloud phase discrimination from a satellite. *IEEE Trans. Geosci. Rem. Sensing Letters*, 3, 103-106.

Kokhanovsky, A.A., de Leeuw, G. 2009a. Satellite Remote Sensing Over Land, Berlin: Springer-Praxis.

Kokhanovsky, A.A., von Hoyningen-Huene, W., Burrows, J.P. 2009b. The determination of the cloud fraction in the SCIAMACHY ground scene using spectral MERIS measurements. *Int. J. Remote Sens.*, 30, 6151-6167.

Kokhanovsky, A.A., Deuzé, J.L., Diner, D.J., Dubovik, O., Ducos, F., Emde, C., Garay, M.J., Grainger, R.G., Heckel, A., Herman, M., Katsev, I.L., Keller, J., Levy, R., North, P.R.J., Prikhach, A.S., Rozanov, V.V., Sayer, A.M., Ota, Y., Tanré, D., Thomas, G.E. and Zege, E.P. 2010. The inter-comparison of major satellite aerosol retrieval algorithms using simulated intensity and polarization characteristics of reflected light. *Atmos. Meas. Tech.*, 3, 909-932.

Kokhanovsky, A.A., Rozanov V.V. 2010. The determination of the dust cloud altitude from a satellite using hyperspectral measurements in the gaseous absorption band. *Int. J. Remote Sens.*, 31, 2729-2744.

Krijger, J.M., Aben, I. and Schrijver, H. 2005. Distinction between clouds and ice/snow covered surfaces in the identification of cloud-free observations using SCIAMACHY PMDs. *Atmos. Chem. Phys.*, 5, 2729-2738.

Kühl, S., Wilms-Grabe, W., Frankenberg, C., Grzegorski, M., Platt, U. and Wagner, T. 2006. Comparison of OClO nadir measurements from SCIAMACHY and GOME. *Adv. Space Res.,* 37, 2247-2253.

Kühl, S., Pukite, J., Deutschmann, T., Platt, U. and Wagner, T. 2008. SCIAMACHY limb measurements of NO_2, BrO and OClO. Retrieval of vertical profiles: Algorithm, first results, sensitivity and comparison studies. *Adv. Space. Res.*, 42, 1747-1764.

Lee, C., Martin, R.V., van Donkelaar, A., O'Byrne, G., Krotkov, N., Richter, A., Huey, G., and Holloways, J.S. 2009. Retrieval of vertical columns of sulfur dioxide from SCIAMACHY and OMI: Air mass factor algorithm development and validation. *J. Geophys. Res.*, 114, D22303, doi:10.1029/2009JD012123.

Lenoble, J. (ed.) 1985. Radiative Transfer in Scattering and Absorbing Atmospheres. Standard Computational Procedures. *A. Deepak Publishing*, Hampton, VA, USA.

Lerot, C., Van Roozendael, M., van Geffen, J., van Gent, J., Fayt, C., Spurr, R., Lichtenberg, G. and von Bargen, A. 2009. Six years of total ozone column measurements from SCIAMACHY nadir observations. *Atmos. Meas. Tech.*, 2, 87-98.

Lichtenberg, G., Bovensmann, H., Van Roozendael, M., Doicu, A., Eichmann, K.-U., Hess, M., Hrechanyy, S., Kokhanovsky, A., Lerot, C., Noël, S., Richter, A., Rozanov, A., Schreier, F. and Tilstra, L.G. 2010. SCIAMACHY Offline Level 1b-2 Processor Algorithm Theoretical Baseline Document (ENV-ATB-QWG-SCIA-0085). *Technical Document*, SQWG/DLR-IMF.
available at http://atmos.caf.dlr.de/sciamachy/documentation.html

Liou, K.N. 2002. An Introduction to Atmospheric Radiation. Academic Press, *International Geophysical Series*, 84.

Lotz, W.A., Vountas, M., Dinter, T. and Burrows, J.P. 2009. Cloud and surface classification using SCIAMACHY polarization measurement devices. *Atmos. Chem. Phys.*, 9, 1279-1288.

Loughman, R.P., Griffioen, E., Oikarinen, L., Postylyakov, O.V., Rozanov, A., Flittner, D.E. and Rault, D.F. 2004. Comparison of radiative transfer models for limb-viewing scattered sunlight measurements. *J. Geophys. Res.*, 109(D6), D06303, doi:10.1029/2003JD003854.

Loyola, D. 1998. A New Cloud Recognition Algorithm for Optical Sensors. *IEEE International Geoscience and Remote Sensing Symposium, IGARSS'98 Digest*, Volume II, 572-574.

Martin, R.V., Chance, K., Jacob, D.J., Kurosu, T.P., Spurr, R.J.D., Bucsela, E., Gleason, J.F., Palmer, P.I., Bey, I., Fiore, A.M., Li, Q., Yantosca, R.M. and Koelemeijer, R.B.A. 2002. An improved retrieval of tropospheric nitrogen dioxide from GOME. *J. Geophys. Res.*, 107, 4437-4456, doi:10.1029/2001JD001027.

McLinden, C.A., McConnell, J.C., Griffioen, E., and McElroy, C.T. 2002. A vector radiative transfer model for the Odin/OSIRIS project, Can. J. Phys., 80:375-393.

Meyer, J., Bracher, A., Rozanov, A., Schlesier, A.C., Bovensmann, H. and Burrows, J.P. 2005. Solar occultation with SCIAMACHY: algorithm description and first validation. *Atmos. Chem. Phys.*, 5, 1589-1604.

Montoux, N., Hauchecorne, A., Pommereau, J.-P., Lefèvre, F., Durry, G., Jones, R. L., Rozanov, A., Dhomse, S., Burrows, J.P., Morel, B. and Bencherif, H. 2009. Evaluation of balloon and satellite water vapour measurements in the Southern tropical and subtropical UTLS during the HIBISCUS campaign. *Atmos. Chem. Phys.*, 9, 5299-5319.

Munro, R., Siddans, R., Reburn, W.J. and Kerridge, B. 1998. Direct measurement of tropospheric ozone from space. *Nature*, 392, 168-171.

Nakajima, T. and King, M.D. 1990. Determination of the optical thickness and effective particle radius of clouds from reflected solar radiation measurements. Part I: Theory. *J. Atmos. Sci.*, 47, 1878-1893.

Noël, S., Buchwitz, M., Bovensmann, H. and Burrows, J.P. 2004. First retrieval of global water vapour column amounts from SCIAMACHY measurements. *Atmos. Chem. Phys.*, 4, 111-125.

Noël, S., Bramstedt, K., Rozanov, A., Bovensmann, H. and Burrows, J.P. 2010. Water vapour profiles from SCIAMACHY solar occultation measurements derived with an onion peeling approach. *Atmos. Meas. Tech.*, 3, 523-535.

Noxon, J.F., 1975. Nitrogen dioxide in the stratosphere and troposphere measured by ground-based absorption spectroscopy. *Science*, 189, 547.

Oetjen, H., Wittrock, F., Richter, A., Chipperfield, M.P., Medeke, T., Sheode, N., Sinnhuber, B.-M., Sinnhuber, M., and Burrows, J.P. 2009. Evaluation of stratospheric chlorine chemistry for the Arctic spring 2005 using modelled and measured OClO column densities. *Atmos. Chem. Phys. Discuss.*, 9, 26539-26575.

Penning de Vries, M., Beirle, S. and Wagner, T. 2009. UV aerosol indices from SCIAMACHY: introducing the SCattering Index (SCI). *Atmos. Chem. Phys.*, 9, 9555-9567.

Platnick, S., King, M.D., Ackerman, S.A., Menzel, W.P., Baum, B.A., Rièdi, J.C. and Frey, R.A. 2003. The MODIS cloud products: Algorithms and examples from Terra. *IEEE Transactions on Geoscience and Remote Sensing*, 41, 459-473.

Platt, U., Perner, D. and Pätz, H.W. 1979. Simultaneous measurements of atmospheric CH_2, O_3 and NO_2 by differential optical absorption. *J. Geophys. Res.*, 84, 6329-6335.

Platt, U. and Stutz, J., 2008. Differential Optical Absorption Spectroscopy: Principles and Applications. *Springer*, Physics of Earth and Space Environments, ISBN 978-3-540-21193-8.

Pöschl, U. 2005. Atmospheric Aerosols: Composition, Transformation, Climate and Health Effects. *Angew. Chem. Int. Ed.*, *44*, 7520-7540.

Puķīte, J., Kühl, S., Deutschmann, T., Platt, U.. and Wagner, T. 2009. Extending differential optical absorption spectroscopy for limb measurements in the UV. *Atmos. Meas. Tech.*, 3, 1155-1174, doi:10.5194/amt-3-1155-2010.

Puķīte, J., Kühl, S., Deutschmann, T., Dörner, S., Jöckel, P., Platt, U., Wagner, T. 2010. The effect of horizontal gradients and spatial measurement resolution on the retrieval of global vertical NO_2 distributions from SCIAMACHY measurements in limb only mode. *Atmos. Meas. Tech.*, 3, 1155-1174, doi:10.5194/amt-3-1155-2010.

Richter, A. and Burrows, J.P. 2002. Retrieval of Tropospheric NO_2 from GOME Measurements. *Adv. Space Res.*, 29, 1673-1683.

Richter, A., Burrows, J.P., Nüß, H., Granier, C. and Niemeier, U. 2005. Increase in nitrogen dioxide over China observed from space. *Nature*, 437, 129-132.

Richter, A., Wittrock, F., and Burrows, J.P. 2006. SO_2 Measurements with SCIAMACHY. *Proc. ESA Atmospheric Science Conference*, Frascati, Italy, ESA SP-628.

Richter, A., Wagner, T. 2011. Solar backscattered radiation: UV, visible and near IR – trace gases. In The Remote Sensing of Tropospheric Composition from Space, eds. J.P. Burrows, P. Borrell and U. Platt, The remote sensing of Tropospheric Composition from Space, Springer Heidelberg Dordrecht London New York, ISBN 978-3-642-14790-6, DOI: 10.1007/978-3-642-14791-3.

Rodgers, C.D. 2000. Inverse Methods for Atmospheric Sounding: Theory and Practice. Series on Atmospheric, Oceanic and Planetary Physics, Vol. 2, World Scientific.

Rohen, G.J., von Savigny, C. Eichmann, K.-U., Llewellyn, E.J., Bracher, A. and Burrows, J.P. 2006. Retrieval of mesospheric ozone profiles from SCIAMACHY limb scattering observations: Theory, first validation results and ozone depletion during the Oct./Nov. 2003 solar proton event. *Adv. Space Res*., 37, 2263–2268, doi:10.1016/j.asr.200503.160.

Rohen, G.J., von Savigny, C., Kaiser, J.W., Llewellyn, E.J., Froidevaux, L., Lopez-Puertas, M., Steck, T., Palm, M., Winkler, H., Sinnhuber, M., Bovensmann, H. and Burrows, J.P. 2008, Ozone profile retrieval from limb scatter measurements in the HARTLEY bands: further retrieval details and profile comparisons. *Atmos. Chem. Phys.*, 8, 2509-2517.

Rozanov, A., Rozanov, V. and Burrows, J.P. 2001. A numerical radiative transfer model for a spherical planetary atmosphere: Combined differential-integral approach involving the Picard iterative approximation. *J. Quant. Spectr. Rad. Transfer*, 69, 491-512.

Rozanov, A., Rozanov, V., Buchwitz, M., Kokhanovsky, A. and Burrows, J.P. 2005a. SCIATRAN 2.0 – A new radiative transfer model for geophysical applications in the 175-2400 nm spectral region. *Adv. Space Res.*, 36, 1015-1019.

Rozanov, A., Bovensmann, H., Bracher, A., Hrechany, S., Rozanov, V., Sinnhuber, M., Stroh, F. and Burrows, J.P. 2005b. NO_2 and BrO vertical profile retrieval from SCIAMACHY limb measurements: sensitivity studies. *Adv. Space Res.*, 36, 846–854.

Rozanov, A., Eichmann, K.-U., von Savigny, C., Bovensmann, H., Burrows, J.P., von Bargen, A., Doicu, A., Hilgers, S., Godin-Beekmann, S., Leblanc, T., and McDermid, I.S. 2007. Comparison of the inversion algorithms applied to the ozone vertical profile retrieval from SCIAMACHY limb measurements, *Atmos. Chem. Phys.*, 7, 4763-4779.

Rozanov, A., Weigel, K., Bovensmann, H., Dhomse, S., Eichmann, K.-U., Kivi, R., Rozanov, V., Vömel, H., Weber, M., and Burrows, J.P. 2010. Retrieval of water vapor vertical distributions in the upper troposphere and the lower stratosphere from SCIAMACHY limb measurements, *Atmos. Meas. Tech. Discuss.*, 3, 4009-4057, doi:10.5194/amtd-3-4009-2010.

Rozanov, V.V., Kurosu, T. and Burrows, J.P. 1998. Retrieval of atmospheric constituents in the UV-visible: A new quasi-analytical approach for the calculation of weighting functions. *J. Quant. Spectr. Rad. Transfer*, 60, 277-299.

Rozanov, V.V. and Kokhanovsky, A.A. 2004. Semi-analytical cloud retrieval algorithm as applied to the cloud top altitude and the cloud geometrical thickness determination from top-of-atmosphere reflectance measurements in the oxygen A-band. *J. Geophys. Res.*, 109, D05202, 10.1029/2003JD004104.

Rozanov, V.V., Rozanov, A.V. 2010. Differential optical absorption spectroscopy (DOAS) and air mass factor concept for a multiply scattering vertically inhomogeneous medium: theoretical consideration. *Atmos. Meas. Tech.*, 3, 751-780.

Saiz-Lopez, A., Chance, K., Liu, X., Kurosu, T.P. and Sander, S.P. 2007. First observations of iodine oxide from space. *Geophys. Res. Letters*, 34, L12812, doi:10.1029/2007GL030111.

Sarkissian, A., Roscoe, H.K. and Fish, D.J. 1995. Ozone measurements by zenith-sky spectrometers: An evaluation of errors in Air Mass Factors calculated by radiative transfer models. *J. Quant. Spectrosc. Radiat. Transfer,* 54, 471-480.

Scharringhausen, M., Aikin, A.C., Burrows, J.P. and Sinnhuber, M. 2008. Global column density retrievals of mesospheric and thermospheric Mg I and Mg II from SCIAMACHY limb and nadir radiance data. *J. Geophys. Res.*, 113, D13303, doi:10.1029/2007JD009043.

Schlundt, C., Kokhanovsky, A.A., von Hoyningen-Huene, W., Dinter, T., Istomina, L. and Burrows J. P. 2010. Synergetic cloud fraction determination from SCIAMACHY using MERIS. *Atmos. Meas. Tech. Discuss.*., 3, 3601-3642.

Schneising, O., Buchwitz, M., Burrows, J.P., Bovensmann, H., Reuter, M., Notholt, J., Macatangay, R. and Warneke, T. 2008. Three years of greenhouse gas column-averaged dry air mole fractions retrieved from satellite - Part 1: Carbon dioxide. *Atmos. Chem. Phys.*, 8, 3827-3853.

Schneising, O., Buchwitz, M., Burrows, J.P., Bovensmann, H., Bergamaschi, P. and Peters, W. 2009. Three years of greenhouse gas column-averaged dry air mole fractions retrieved from satellite - Part 2: Methane. *Atmos. Chem. Phys.*, 9, 443-465.

Schönhardt, A., Richter, A., Wittrock, F., Kirk, H., Oetjen, H., Roscoe, H.K. and Burrows, J.P. 2008. Observations of iodine monoxide (IO) columns from satellite. *Atmos. Chem. Phys.*, 8, 637-653.

Schreier, F., Gimeno-Garcia, S., Hess, M., Doicu, A. and Lichtenberg, G. 2009. Carbon monoxide vertical column density retrieval from SCIAMACHY infrared nadir observations. In IRS 2008: Current Problems in Atmospheric Radiation, eds. T. Nakajiama and M.A. Yamasoe, *American Institute of Physics*, doi: 10.1063/1.3116983.

Schrijver, H., Gloudemans, A.M.S., Frankenberg, C. and Aben, I. 2009. Water vapour total columns from SCIAMACHY spectra in the 2.36 μm window. *Atmos. Meas. Tech.*, 2, 561-571.

Sierk, B., Richter, A., Rozanov, A., von Savigny, C., Schmoltner, A.M., Buchwitz, M., Bovensmann, H. and Burrows, J.P. 2006. Retrieval and Monitoring of atmospheric trace gas concentrations in nadir and limb geometry using the space-borne SCIAMACHY instrument. *Environ. Mon. Assess.*, doi: 10.1007/s10661-005-9049-9.

Sioris, C.E., Kurosu, T.P., Martin, R.V. and Chance, K. 2004. Stratospheric and tropospheric NO_2 observed by SCIAMACHY: First results. *Adv. Space Res.*, 34, 780-785.

Sioris, C.E., Kovalenko, L.J., McLinden, C.A., Salawitch, R.J., Van Roozendael, M., Goutail, F., Dorf, M., Pfeilsticker, K., Chance, K., von Savigny, C., Liu, X., Kurosu, T.P., Pommereau, J.-P., Bösch, H. and Frerick, J. 2006. Latitudinal and vertical distribution of bromine monoxide in the lower stratosphere from Scanning Imaging Absorption Spectrometer for Atmospheric Chartography limb scattering measurements. *J. Geophys. Res.*, 111, D14301, doi:10.1029/2005JD006479.

Slijkhuis, S., von Bargen, A., Thomas, W. and Chance, K. 1999. Calculation of undersampling correction spectra for DOAS spectral fitting. *Proc Atmospheric Measurements from Space – ESAMS '99*, Noordwijk, The Netherlands, WPP-161 563-569.

Solomon, S., Schmeltekopf, A.L. and Sanders, R.W. 1987. On the interpretation of zenith sky absorption measurements. *J. Geophys. Res.*, 92, 8311-8319.

Sonkaew, T., Rozanov, V.V., von Savigny, C., Rozanov, A., Bovensmann, H. and Burrows, J.P. 2009. Cloud sensitivity studies for stratospheric and lower mesospheric ozone profile retrievals from measurements of limb-scattered solar radiation. *Atmos. Meas. Tech.*, 2, 653-678.

Spurr, R.J.D., Kurosu, T.P. and Chance, K.V. 2001. A linearized discrete ordinate radiative transfer model for atmospheric remote-sensing retrieval. *J. Quant. Spect. Rad. Transfer*, 68, 689-735.

Stammes, P. 2001. Spectral radiance modelling in the UV-Visible range. In IRS 2000: Current problems in Atmospheric Radiation, eds. W.L. Smith and Y.M. Timofeyev, *A. Deepak Publ.*, Hampton, VA, 385-388.

Thomas, G.E. and Stamnes, K. 1999. Radiative transfer in the atmosphere and ocean. *Cambridge: Cambridge University Press*.

Torres, O., Bhartia, P.K., Herman, J.R., Ahmad, Z. and Gleason, J. 1998. Derivation of aerosol properties from satellite measurements of backscattered UV radiation: Theoretical basis. *J. Geophys. Res.* 103(D14), 17099-17110.

Vassilkov, A.P., Joiner, J., Gleason, J. and Bhartia, P. 2002. Ocean Raman scattering in satellite backscatter UV measurements. *Geophys. Res. Let.*, 10, 1837-1840.

Velders, G.J.M., Granier, C., Portmann, R.W., Pfeilsticker, K., Wenig, M., Wagner, T., Platt, U., Richter, A. and Burrows, J.P. 2001. Global tropospheric NO_2 column distributions: Comparing 3-D model calculations with GOME measurements. *J. Geophys. Res.*, 106, 12643-12660.

von Hoyningen-Huene, W., Freitag, M. and Burrows, J.P. 2003. Retrieval of aerosol optical thickness over land surfaces from top-of-atmosphere radiance. *J. Geophys. Res.*, 108, doi:10.1029/2001JD002018.

von Hoyningen-Huene, W., Kokhanovsky, A.A., Wuttke, M., Buchwitz, M., Noël, S., Gerilowski, K., Burrows, J.P., Latter, B., Siddans, R. and Kerridge, B.J. 2007. Validation of SCIAMACHY top-of-atmosphere reflectance for aerosol remote sensing using MERIS L1 data. *Atmos. Chem. Phys.*, 7, 97-106 .

von Savigny, C., Kokhanovsky, A., Bovensmann, H., Eichmann, K.-U., Kaiser, J.W., Noël, S., Rozanov, A.V., Skupin, J. and Burrows, J.P. 2004a. NLC Detection and Particle Size Determination: First Results from SCIAMACHY on ENVISAT. *Adv. Space Res.*, 34, 851-856.

von Savigny, C., Eichmann, K.-U., Llewellyn, E.J., Bovensmann, H., Burrows, J.P., Bittner, M., Höppner, K., Offermann, D., Steinbrecht, W., Winkler, P., Taylor, M.J. and Cheng, Y. 2004b. First near-global retrieval of OH rotational temperatures from satellite-based Meinel band emission measurements. *Geophys. Res. Lett.*, 31, L15111, doi:10.1029/2004GL.

von Savigny, C., Rozanov, A., Bovensmann, H., Eichmann, K.-U., Noël, S., Rozanov, V.V., Sinnhuber, B.-M., Weber, M. and Burrows, J.P. 2005a. The ozone hole break-up in September 2002 as seen by SCIAMACHY on ENVISAT. *J. Atmos. Sci.*, 62, 721-734

von Savigny, C., Ulasi, E.P., Eichmann, K.-U., Bovensmann, H. and Burrows, J.P. 2005b. Detection and Mapping of Polar Stratospheric Clouds using Limb Scattering Observations. *Atmos. Chem. Phys.*, 5, 3071-3079.

Vountas, M., Rozanov, V. and Burrows, J. 1998: Ring effect: Impact of rotational Raman scattering on radiative transfer in earth's atmosphere. *J. Quant. Spectrosc. Radiat. Transfer*, 60, 943-961.

Vountas, M., Dinter, T., Bracher, A., Burrows, J.P. and Sierk, B. 2007. Spectral Studies of Ocean Water with Space-borne Sensor SCIAMACHY using Differential Optical Absorption Spectroscopy (DOAS). *Ocean Sci.*, 3, 429-440.

Vrekoussis, M., Wittrock, F., Richter, A. and Burrows, J.P. 2009. Temporal and spatial variability of glyoxal as observed from space. *Atmos. Chem. Phys.*, 9, 4485-4504.

Wagner, T., Burrows, J.P., Deutschmann, T., Dix, B., von Friedeburg, C., Frieß, U., Hendrick, F., Heue, K.-P., Irie, H., Iwabuchi, H., Kanaya, Y., Keller, J., McLinden, C.A., Oetjen, H., Palazzi, E., Petritoli, A., Platt, U., Postylyakov, O., Pukite, J., Richter, A., van Roozendael, M., Rozanov, A., Rozanov, V., Sinreich, R., Sanghavi, S. and Wittrock, F. 2007a. Comparison of Box-Air-Mass-Factors and Radiances for Multiple-Axis Differential Optical Absorption Spectroscopy (MAX-DOAS) Geometries calculated from different UV/visible Radiative Transfer Models. *Atmos. Chem. Phys.*, 7, 1809-1833.

Wagner, T., Beirle, S., Deutschmann, T., Grzegorski, M. and Platt, U. 2007b. Satellite monitoring of different vegetation types by differential optical absorption spectroscopy (DOAS) in the red spectral Range. *Atmos. Chem. Phys.*, 7, 69-79.

Wagner, T., Beirle, S., and Deutschmann, T. 2009. Three-dimensional simulation of the Ring effect in observations of scattered sun light using Monte Carlo radiative transfer models, *Atmos. Meas. Tech.*, 2, 113-124.

Wang, P. Stammes, P., van der A, R., Pinardi, G. and Van Roozendael, M. 2008. FRESCO+: an improved O_2 A-band cloud retrieval algorithm for tropospheric trace gas retrievals. *Atmos. Chem. Phys.*, 6565-6576.

Weber, M., Lamsal, L.N., Coldewey-Egbers, M., Bramstedt, K. and Burrows, J.P. 2005. Pole-to-pole validation of GOME WFM-DOAS total ozone with groundbased data. *Atmos. Chem. Phys.*, 5, 1341-1355.

Wittrock F., Richter, A., Oetjen, H., Burrows, J.P., Kanakidou, M., Myriokefalitakis, S., Volkamer, R., Beirle, S., Platt, U., Wagner, T. 2006. Simultaneous global observations of glyoxal and formaldehyde from space. *Geophys. Res. Lett.*, 33, L16804, doi:10.1029/2006GL026310.

Yamamoto, G,A. and Wark, D.Q. 1961. Discussion of the letter by R.A. Hanel: Determination of cloud altitude from satellite. *J. Geophys. Res.*, 66, 3596.

Yan, X. 2005. A fast SCIAMACHY PMD Cloud Algorithm (SPCA). *Master Thesis*, University of Bremen.
available at http://www.iup.uni-bremen.de/doas/paper/yang_thesis_spca_0509.pdf